Investigation of Pressurized Fluidization with Novel Borescopic Particle Image Velocimetry

Dellaert, R.A.

Award date:
2016

Technische Universiteit
Eindhoven
University of Technology

Process Engineering
Multiphase Reactor group (SMR)
Department of Chemical Engineering and Chemistry

Den Dolech 2, 5612 AZ Eindhoven
P.O. Box 513, 5600 MB Eindhoven
The Netherlands
www.tue.nl

Author:
R.A. Dellaert (ID: 0772091)

Graduation Committee:
Prof. Dr. Ir. J.A.M. Kuipers (chair)
Prof. Dr. J. Meuldijk (external)
Prof. Dr. ir. N.G.Deen (supervisor)
M. Banaei MSc. (tutor)

Date:
May 2016

Version:
FINAL

Investigation of Pressurized Fluidization with Novel Borescopic Particle Image Velocimetry

R.A. Dellaert
May 2016

Contents

Abstract

To get a better understanding of the hydrodynamics of a pressurized fluidized bed, a novel technique was developed, validated and used. This novel technique is the Borescopic particle image velocimetry (BPIV).

The novel BPIV technique has been validated with various experimental tests to check its applicability for bubbling gas-solid fluidized beds. It was found that the BPIV results are in fair agreement with positron emission particle tracking (PEPT) results at velocities well above minimum fluidization velocity, although there is an intrusiveness effect. Besides that the optimum settings for BPIV measurements was determined too. The best camera settings among the investigated settings, especially for high superficial gas velocities, are 1000 FPS with an exposure time of 992 μs and a minimum of 7500 frames (=7.5 s).

After successfully validating the experimental method, the BPIV was used to measure the average particle velocity profile for various pressures between 1 to 16 bara. It was found that the average particle velocity shows an up-going movement near the center of the fluidized bed and an average velocity around zero near the wall of the bed. During the experiments it was observed that the frequency of the bubbles near the center of the fluidized bed was much higher than near the wall regions.

Besides the experimental part of this project, the two fluid model was also used for finding the effect of pressure on fluidization. After processing the results, it is found that the TFM gives comparable outcomes to the existing results in open literature. It was found that the operating pressure has an effect on the fluidization behavior. As the simulations were performed with an aspect ratio of 0.5 and experiments were performed with an aspect ratio of 1.0, it is not possible to compare their results to each other.

Nomenclature

Symbols, their definitions and their units		
Ar	Archimedes number	-
C_d	Drag coefficient	-
c_p	Particle velocity	m/s
C_p	Velocity fluctuation component	m/s
d	Diameter	m
dt	Time step	s
e	Restitution coefficient	-
$f(\varepsilon)$	Porosity function	-
g	Gravitational constant	m/s^2
g_0	Radial distribution function	-
h	Height	m
I	Moment of inertia	$kg \cdot m^2$
M	Molar mass	kg/mol
P	Pressure	Pa
q	Pseudo-Fourier fluctuating kinetic energy flux	kg/s^3
R	Gas constant	J/(K·mol)
Re	Reynolds number	-
t	Time	s
T	Temperature	K
u	Gas phase velocity	m/s
v	Particle velocity	m/s
V	Volume	m^3

Greek symbols, their definitions and their units		
β	Interphase momentum transfer coefficient	$kg/(m^3 \cdot s)$
γ	Dissipation of granular energy	$kg/(m \cdot s^3)$
ε	Porosity	-
θ	Granular temperature	m^2/s^2
κ	Pseudo-thermal conductivity	kg/(m·s)
λ	Bulk viscosity	Pa·s
μ	Dynamic viscosity	Pa·s
ρ	Density	kg/m^3
$\bar{\bar{\tau}}$	Stress tensor	$kg/(s^2 \cdot m)$

Operators and their definitions	
∇	Gradient
$\nabla \cdot$	Divergence

Subscripts and their definitions	
f	Fluid
g	Gas
mf	Minimum fluidization
p	Particle
s	Solid

Abbreviations and their definitions	
2D	Two dimensional
3D	Three dimensional
BPIV	Borescopic particle image velocimetry
CFD	Computational fluid dynamics
DIA-PIV	Digital image analysis-particle image velocimetry
DNS	Direct numerical simulation
DBM	Discrete bubble model
DPM	Discrete particle model
ECT	Electrical capacitance tomography
FBR	Fluidized bed reactors
FPS	Frames per second
KTGF	Kinetic Theory of Granular Flow
LBM	Lattice Boltzmann model
LLDPE	Linear low density polyethylene
PDF	Probability distribution function
PEPT	Positron emission particle tracking
RAM	Random-access memory
RPM	Revolutions per minute
RPT	Radioactive particle tracking
THM	Temporal histogram method
TFM	Two-fluid model

1 Introduction

Fluidization is a process where the gravity force that is exerting on the particles is lower or in equilibrium with the friction force of the up going gas or liquid. Consequently, the particles start to flow and act like a fluid in this process. A schematic representation of a fluidized bed reactor can be found in figure 1.

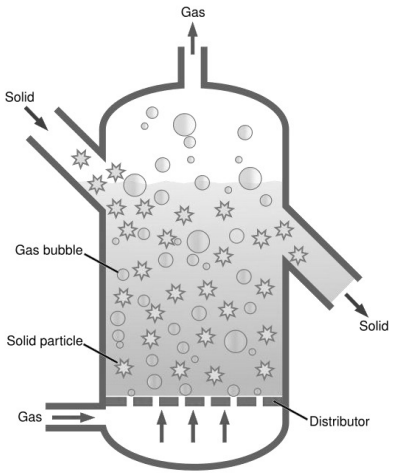

Figure 1: Example of a fluidized bed reactor [1].

1.1 Fluidized beds applications

Fluidized beds are widely used in petroleum and petrochemical industries for producing a various range of products like jet fuel, synthetic fibers, fertilizers and different polymers (i.e.: polyethylene, polypropylene, polyvinyl chloride, styrene, and rubber) [2].

Fluidized bed reactors (FBR) are quite novel in the process industry and have their advantages and disadvantages compared to other conventional reactor types.
Some of the advantages of these reactors are:

- Good mixing of the particles and high heat transfer rate that leads to a uniform temperature distribution in the bed.
- A continuous steady state operation which can be easily controlled.
- It can be used in large productions.
- The mass transfer rate between the fluid and the particles is relatively high.

The disadvantages are:

- The gas or liquid that flows through the fluidized bed, needs to be pumped into the reactor because the particles cause a pressure drop. This pressure drop is quite considerable and a lot of energy is required to overcome it.
- Particles can get pulverized due to friction with other particles and entrained by the fluid.
- Damage on the reactor and pipes due to friction of the particles can occur (erosion).
- Due to complexity of heat and mass-transfer properties these phenomena in fluidized beds are not fully understood at this moment [3].

1.2 Previous research

In the past, there has been a lot of research on fluidization. Link [4] did a research on spout-fluid beds where large particles are in contact with a gas. Van der Schaaf et al. [5] studied the pressure waves and pressure fluctuations in bubbling gas-solid fluidized beds. Godlieb [6] did an experimental and modeling research with the Two-Fluid Model (TFM) and the discrete particle model (DPM) on pressurized fluidized beds. Gorter et al. [7] studied the bubble characteristics in a pressurized fluidized bed with electrical capacitance tomography measurements. Hoomans et al. [8] developed a hard-sphere discrete particle model of a gas-fluidized bed where the motion of the particles was predicted from the acting forces. Laverman [9] investigated the hydrodynamics and solid circulation patterns in a fluidized bed filled with linear low density polyethylene (LLDPE) and glass particles. He also performed various experiments with LLDPE and glass particles with positron emission particle tracking (PEPT). Besides that Laverman [9] used digital image analysis-particle image velocimetry (DIA-PIV) techniques too.

All the aforementioned techniques are conventional methods. On the other hand, new experimental techniques can give a new insight on the complex behavior of fluidized beds. Recently, Tebianian et al. [10] compared four particle velocity measurement techniques in a fluidized bed. Namely two non-intrusive techniques; radioactive particle tracking (RPT) and positron emission particle tracking (PEPT) and two intrusive techniques; the optical fiber probes and the borescopic high speed particle image velocimetry. The borescopic high speed particle image velocimetry is very similar to the method that is used in this project.

Hoeben [11] and Oldeman [12] both worked with the same fluidized bed that is used in this project. Hoeben [11] did a study on the effect of the restitution coefficient, pressure, and particle diameter in a gas fluidized bed simulated with the TFM making use of the Kinetic theory of granular flow (KTGF) simulation technique. He compared his findings with results found by applying the electrical capacitance tomography (ECT) experimental technique. Oldeman [12] used the same borescope that is used in this project to do experiments on the hydrodynamics of a bubbling gas-solid fluidized bed under atmospheric conditions. He also tried to find a correlation between solid velocity and bubble velocity based on the simulation results.

1.3 Research goal

As previously mentioned in this report, one of the biggest disadvantages of fluidized beds is that there are a lot of phenomena inside a fluidized bed that are not fully understood yet. Therefore there is a need to investigate these phenomena to nullify this disadvantage. One of the important parameters in fluidized beds is the particle phase velocity, which is being researched in this project. The moving pattern of the particles shows their mixing rate and mixing pattern in a fluidized bed. This mixing plays an important role to the mass-transfer and heat-transfer. This information plays a key role for designing of a fluidized bed.

The research goal in this project is to get a better understanding of the hydrodynamics of fluidized beds at elevated pressures. The TFM in this project is used for modeling and the borescopic particle image velocimetry (BPIV) is used for the experiments. The BPIV is a novel intrusive technique which can be used under elevated pressures. Via this technique it is possible to look inside of a fluidized bed even during its operation.

1.4. Outline

After this chapter, some literature review and the research goal is presented. This report will continue in chapter two, where the structure of the setup is explained. This setup has a relatively large diameter (0.30 m). The capturing of the data is done with a high speed camera. In chapter three the BPIV technique is tested and the best way that the data could be captured is explored. After that, in chapter four the effect of pressure is presented and discussed. In chapter five the simulations and their corresponding results are presented. Finally, the main conclusions of this work is briefly presented as chapter six.

2 The setup of the experiment

It is necessary to validate BPIV technique before making use of it. In this chapter an explanation is given about the setup and how the BPIV is validated. First the structure of the setup and the borescope is explained. After that, the validation procedure and some additional ideas are discussed. At the end, the results and conclusions are given.

2.1 Structure of the setup

While many other experiments have been done on pseudo-2D fluidized bed. This research is on a large lab-scale three dimensional (3D) fluidized bed. This experimental setup can be operated till 16 bara. As many of the industrial fluidized beds are operated at elevated pressures, this lab-scale setup can mimic these processes. The downside of an elevated pressure are the material requirements. The vessel has to withstand a higher pressure and therefore has to be made of a stronger material, which in this project is steel and it is not transparent. Thus, it is not possible to see the particle's movement from the outside of the fluidized bed.

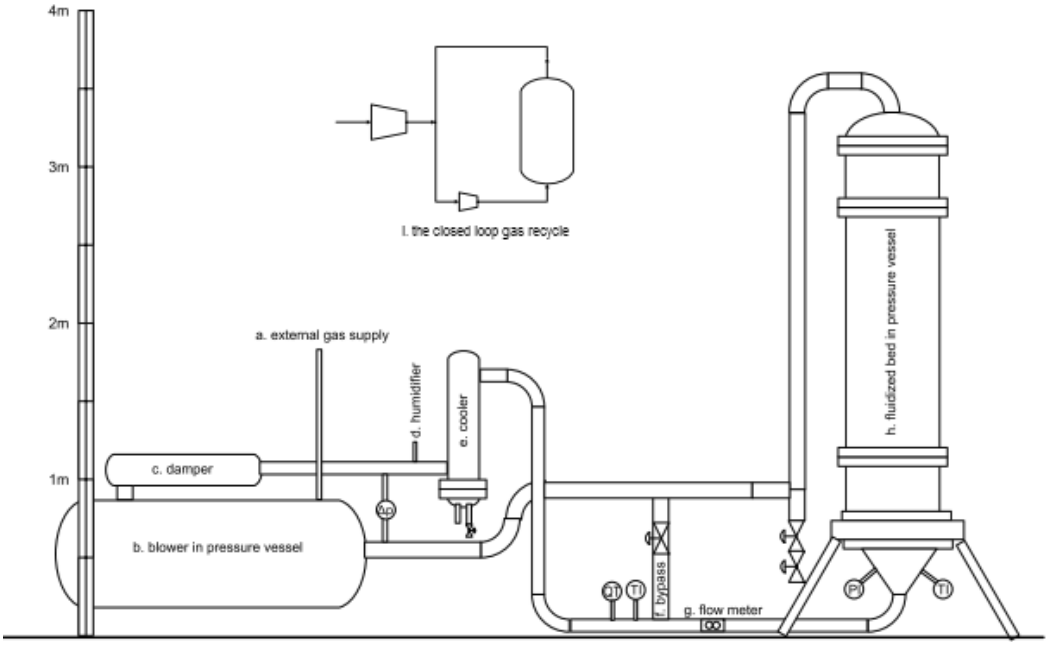

Figure 2: Schematic representation of the fluidized bed setup [12].

In figure 2 the setup that is used for this project is schematically shown. Part (a) can be used to put nitrogen inside the closed system. Part (b) is the blower with part (c), a damper, on top of it. Part (d) is a water pump for humidifying of the fluidizing agent. Part (e) is another safety precautions that can cool the gas inside the system to prevent overheating, but has not been used in this project due to negligible heat production. A bypass and flowmeter are presented in part (f) and part (g), respectively. The fluidized bed is presented in part (h). Where the outer hull exist out of a steel vessel and inside is a polyvinyl chloride cylinder installed, with an internal diameter of 0.306 meter. Inside this cylinder the fluidization takes place. Part (i) shows the closed loop of the gas for recycling.

2.2 Structure and specifications of the borescope

The borescope is placed inside the fluidized bed and is used to take pictures from the experiments. The specifications of the borescope and fluidized bed that are used in this project are shown in table 1 and table 2, respectively.

The top lid of the fluidized bed with the inserted borescope is presented in figure 3. Where part (a) is the lid of the fluidized bed. Part (b) is the high speed camera that is connected to a relatively fast computer. Part (c) is the input for the light source. Part (d) is the borescope. Borescope consists of a lot of lenses for image transfer and it also consists of a light guidance probe. Part (e) is the ocular with a glass plate on top of it (part f) to emit and capture the light back to the borescope.

The computer that is connected to the high speed camera, part (b), needs to be fast enough to save the large amount of data that high speed camera generates and to process these pictures with MATLAB and DaVis programs. The specifications of this computer can be found in table 21.

Table 1: Specifications of the borescope.

Dimensions borescope	
Stick diameter	$1.6 \cdot 10^{-2}$ m
Stick length	1.8 m
Ocular-holder depth	$7.03 \cdot 10^{-2}$ m
Ocular-holder height	$8.0 \cdot 10^{-2}$ m
Ocular-holder width	$2.2 \cdot 10^{-2}$ m
Ocular glass plate height	$5.0 \cdot 10^{-2}$ m
Ocular glass plate width	$1.2 \cdot 10^{-2}$ m

Table 2: Specifications of the fluidized bed.

Dimensions of the fluidized bed and particles	
Inner bed diameter	0.306 m
Particle type	Deco Beads – 45015-427-WI pearl ice [13]
Particle diameter size range	$4.0 \cdot 10^{-4}$ – $06.0 \cdot 10^{-4}$ m
Particle density	2,500 kg/m^3 [14]

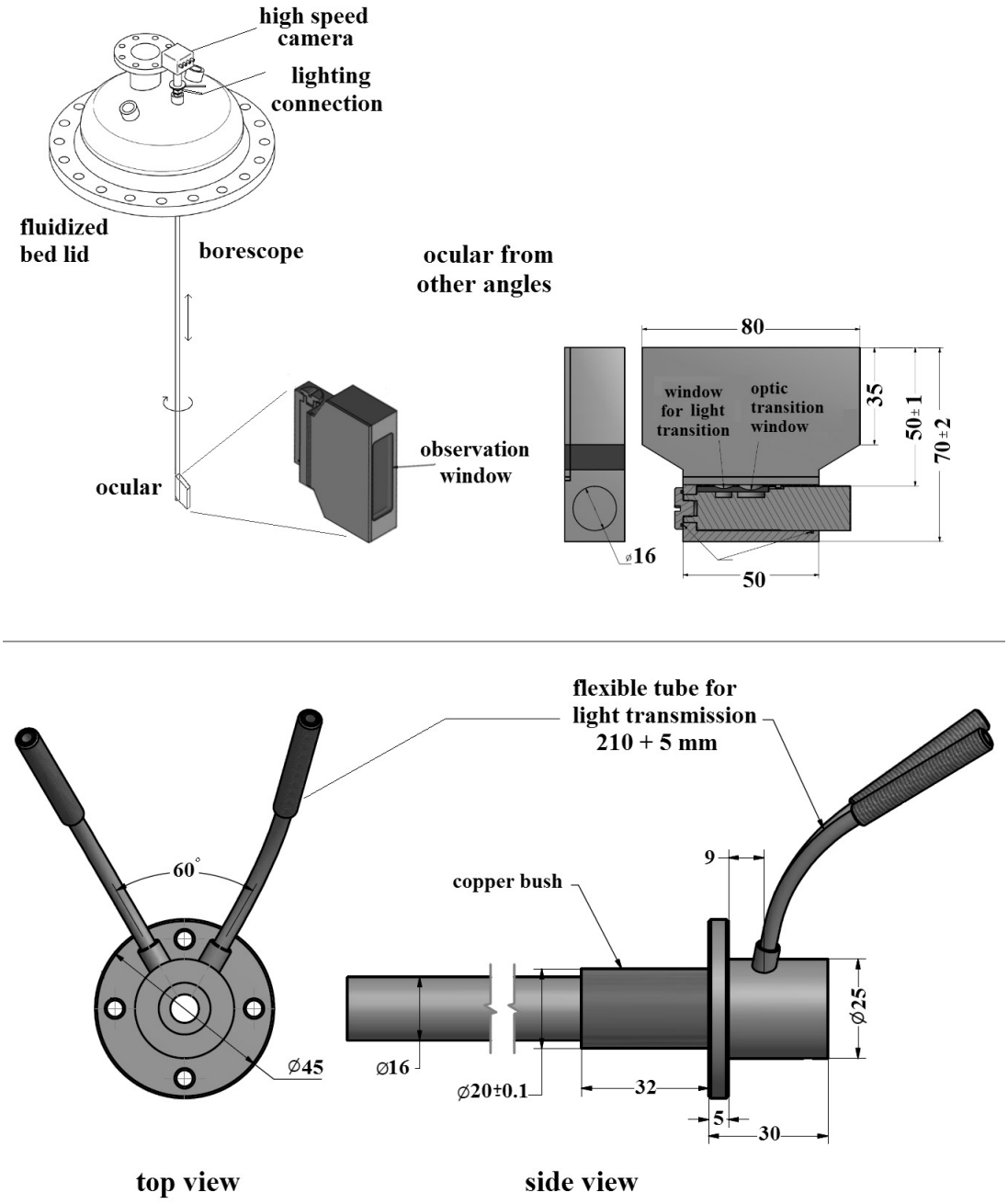

Figure 3: Schematic representation of the top lid of the fluidized bed, the camera, the borescope and the ocular. All the dimensions are in mm.

3 Validation of BPIV technique

In this chapter BPIV validation via various experimental tests is discussed. Besides that, the best settings for using of this technique is presented too. The first performed validation test is 'rotating drill test' which is explained in the following section.

3.1 Rotating drill test

The first way that the BPIV results is tested, is by using a rotating drill. This test only shows the accuracy of BPIV analysis together with the DaVis software package without including the intrusiveness of borescope in fluidized beds. A flat drill head is painted black and white particles are glued to this black surface. The particles that are used in this tests are ordered from the Sigmund-Lindner Company with product type of 45015-427-WI. This drill head is shown in figure 4. The 45015-427-WI particles are opaque with a shining white color and have a diameter between 0.4 and 0.6 mm. It should be noted that the same particle types were used in the final experiments. After gluing all the particles to the drill-head, the drill was positioned in a way that the center of the drill head was exactly in front of the ocular. The rotating drill had a control unit that gave us the possibility to fix its rotational speed.

First a test was done to compare the revolutions per minute (RPM) that was set, with the RPM that was manually counted. As it can be seen in table 3, the actual RPM was a little higher than the RPM that was set. The lowest possible speed of the rotating drill was 10 RPM. Both the 10 and 20 RPM setting showed a higher deviation than the other values. For this reason, these values are not taken into account and the average actual RPM is 9% higher than the RPM that has been set. This slightly higher RPM will be taken into account for all the following calculations.

Table 3: Test results for the controlling device that sets the RPM.

Set RPM	Number of rounds	Time [s]	Real RPM	Deviation
10	10	49.15	12.2	22%
20	20	53.14	22.6	13%
30	30	54.51	33.0	10%
40	40	55.30	43.4	8%
50	50	55.37	54.2	8%
60	60	55.20	65.2	9%
70	70	55.32	75.9	8%
80	80	55.14	87.1	9%
90	90	54.80	98.5	9%
100	100	55.22	108.7	9%

After testing the speed of the rotating drill, the center of the drill head was put in front of the ocular. This is shown on the left side of figure 4. The rotating drill was set on a fixed speed and a series of test were performed with the high speed camera. Then, the produced images were

processed with the program DaVis version 8.2.3. An example of the produced images and a processed images with DaVis can be seen in figure 5. Before processing the images with DaVis, the images were cropped and resized to 50% of their original size to satisfy the necessary conditions of recognition and processing of DaVis.

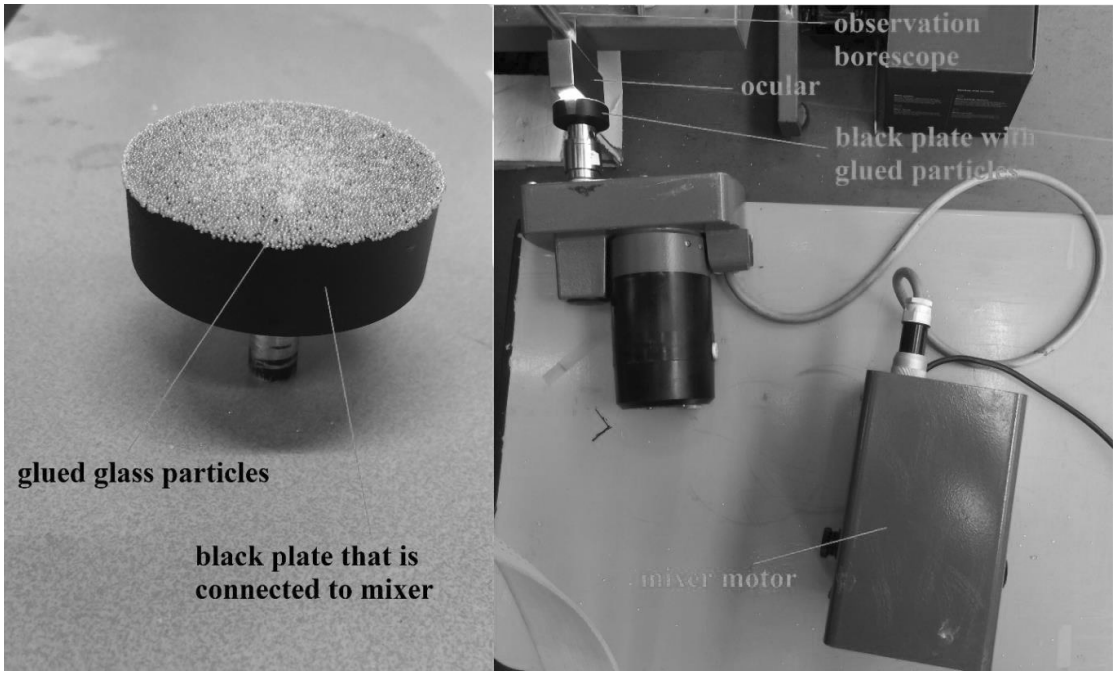

Figure 4: Left: Flat drill head that is painted black with glued white shining 45015-427-WI particles on it. Right: The drill with flat head, the ocular and the drill's motor.

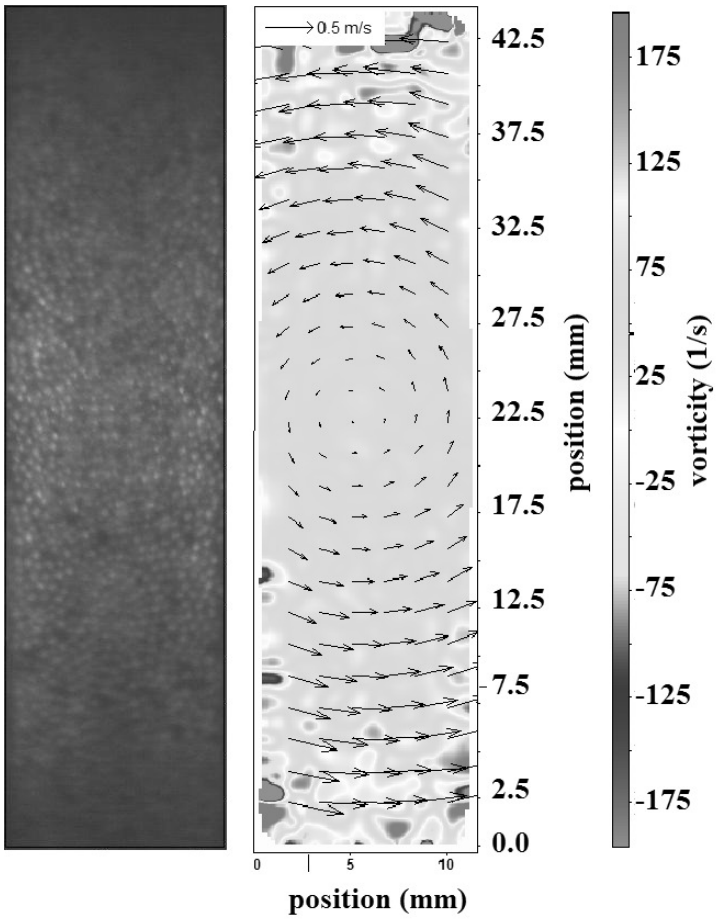

Figure 5: On the left an image is shown that is taken by the camera with a set drill speed of 250 RPM, 992 µm exposure time and 1000 FPS. On the right this image is processed by DaVis. Where the background colors of the image on the right are the vorticity.

The processed images are then converted to Files with the extension of 'vc7', which can be processed by MATLAB. A MATLAB script has been made that can compare the created vc7 files with the actual velocity of the glued particles. In table 4 the results of the rotating drill test at 500 RPM and an exposure time of 1992 µs is given, where table 5 shows the deviation between measured and calculated velocity values. In table 6 the results of the rotating drill test at 1000 RPM and an exposure time of 992 µs is given, where table 7 shows the deviation between measured and calculated values.

In figure 6, figure 7 and figure 8 the theoretical velocity is compared with the measured velocity, with a rotating speed of 10, 100 and 750 RPM, respectively. The origin is not in the middle due to manually placing the ocular in the middle of the drill. This effect has been taken into account in the error calculations.

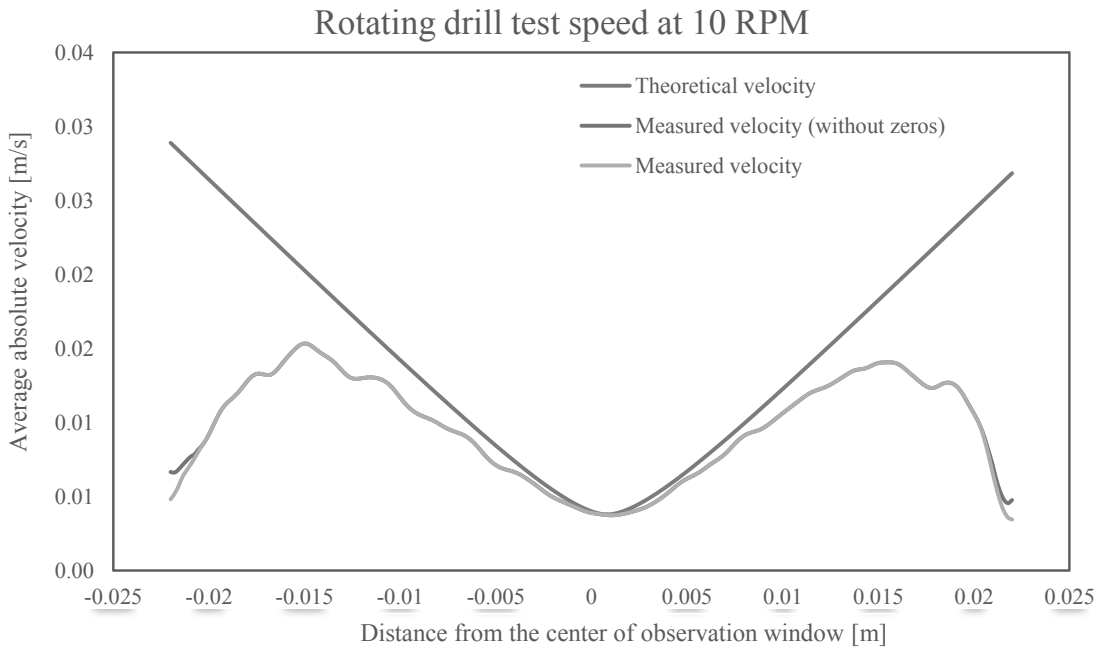

Figure 6: Rotating drill test speed at 10 RPM. Comparison between the theoretical velocity and measured velocities.

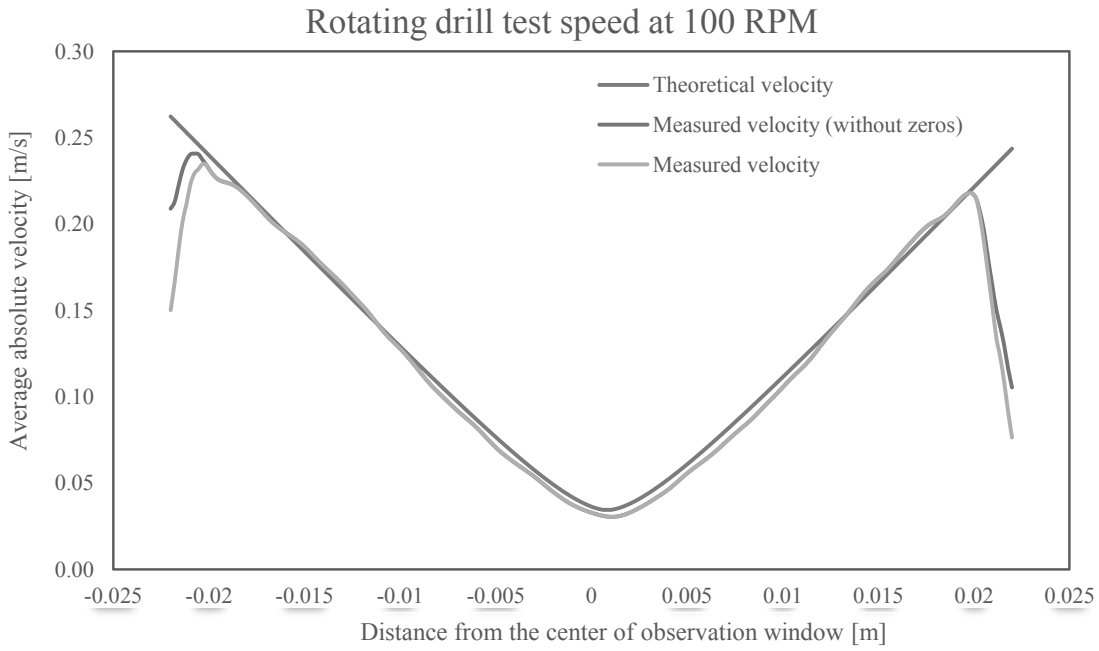

Figure 7: Rotating drill test speed at 100 RPM. Comparison between the theoretical velocity and measured velocities.

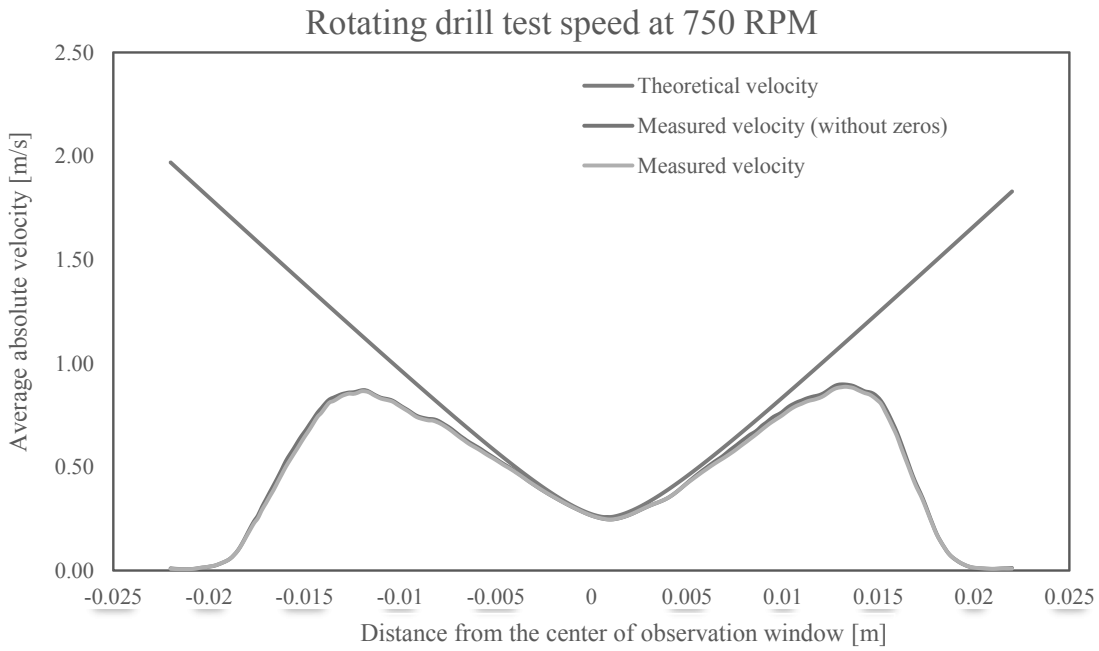

Figure 8: Rotating drill test speed at 750 RPM. Comparison between the theoretical velocity and measured velocities.

The relative deviation of obtained velocities can be found in table 5 and table 7. The obtained velocities have an average relative deviation of 22% and 21% for 500 FPS and 1000 FPS measurements, respectively. When the rotational drill speed is very low, a high relative deviation is noticed. This is probably due to rounding by DaVis. When the rotational drill speed is very high, a high relative deviation is also noticed. This is probably due to blurring of the photo, because of the high velocity of the glued particles. In all the aforementioned analysis, the DaVis processing had an interrogation area of 24 x 24 pixels and an 87% overlap.
Using different image frequencies, leaded to different results. At a low FPS the light intensity increases due to relatively long exposure time. Therefore, brighter images will be obtained. On the other hand, high image frequency settings results in less blurring images compared to low image frequency settings.

Table 4: Results from DaVis with 500 FPS and an exposure time of 1992 µs.

Real drill speed [RPM]	Set drill speed [RPM]	Average theoretical calculated velocity [cm/s]	Average measured velocity [cm/s]	Average measured velocity in x-direction [cm/s]	Average measured velocity in y-direction [cm/s]
12	10	1.85	1.23	1.13	0.36
55	50	8.47	6.63	6.20	1.66
109	100	16.79	12.90	12.04	3.26
273	250	42.06	29.03	26.93	7.34
545	500	83.96	30.98	25.92	11.74
818	750	126.02	29.39	22.68	13.59

Table 5: Results from DaVis with 500 FPS and an exposure time of 1992 µs.

Real drill speed [RPM]	Relative deviation in velocity [%]	Relative deviation in velocity in x-direction [%]	Relative deviation in velocity in y-direction [%]	Absolute deviation in velocity [cm/s]	Absolute deviation in velocity in x-direction [cm/s]	Absolute deviation in velocity in y-direction [cm/s]
12	24%	35%	57%	0.36	0.36	0.13
55	5%	6%	18%	0.30	0.30	0.22
109	4%	6%	17%	0.57	0.59	0.41
273	9%	11%	19%	3.68	3.76	1.38
545	37%	44%	62%	35.34	38.56	9.04
818	53%	60%	75%	70.65	74.33	17.06

Table 6: Results from DaVis with 1000 FPS and an exposure time of 992 µs.

Real drill speed [RPM]	Set drill speed [RPM]	Average theoretical calculated velocity [cm/s]	Average velocity [cm/s]	Average velocity in x-direction [cm/s]	Average velocity in y-direction [cm/s]
12	10	1.85	0.96	0.87	0.32
55	50	8.47	4.66	4.23	1.55
109	100	16.79	12.60	11.83	3.00
273	250	42.06	31.16	29.10	7.64
545	500	83.96	48.64	44.49	13.13
818	750	126.02	47.75	41.25	16.78

Table 7: Results from DaVis with 1000 FPS and an exposure time of 992 µs.

Real drill speed [RPM]	Relative deviation in velocity [%]	Relative deviation in velocity in x-direction [%]	Relative deviation in velocity in y-direction [%]	Absolute deviation in velocity [cm/s]	Absolute deviation in velocity in x-direction [cm/s]	Absolute deviation in velocity in y-direction [cm/s]
12	33%	44%	70%	0.56	0.56	0.16
55	24%	26%	38%	2.07	2.06	0.43
109	9%	10%	27%	1.15	1.13	0.64
273	6%	8%	22%	2.22	2.22	1.36
545	18%	20%	29%	17.98	18.31	4.76
818	35%	39%	49%	52.12	53.77	11.82

It should be noted that in table 4, table 5, table 6 and table 7, the velocity in the x-direction is the velocity in the horizontal direction and the y-direction is in the vertical direction. The average theoretical calculated velocity is higher than the average measured velocity, this is due to some measured velocities in the corners of the pictures, where the velocity is relatively high and could not be calculated. For this reason, these parts are not taken into account for further analysis. These results have been filtered out for the average measured velocity and relative

and absolute deviations, but they are not filtered out for the average theoretical calculated velocity.

3.1.1 Conclusion

The results of the rotating drill test showed an average relative deviations for velocity calculations of 22% at 500 FPS and 21% at 1000 FPS respectively. 500 FPS has a better performance in situations where particles move slowly whereas the 1000 FPS performs better in situations where particles move with larger velocities.

3.1.2 Black particles

Another idea was to decrease the influence of the surrounding white particles in the rotating drill test. This was done by creating a mix of around 90 vol% black and 10 vol% white particles, where the white particles were much clearer and thus easier to track by DaVis. This mixture of white and black particles was created and put on the drill head, just like the rotating drill test which is explained earlier in this chapter. After the first pictures were taken, see figure 9, the conclusion was easy to make. Having a mixture of black and white particles does not increase the accuracy for solid velocity measurement.

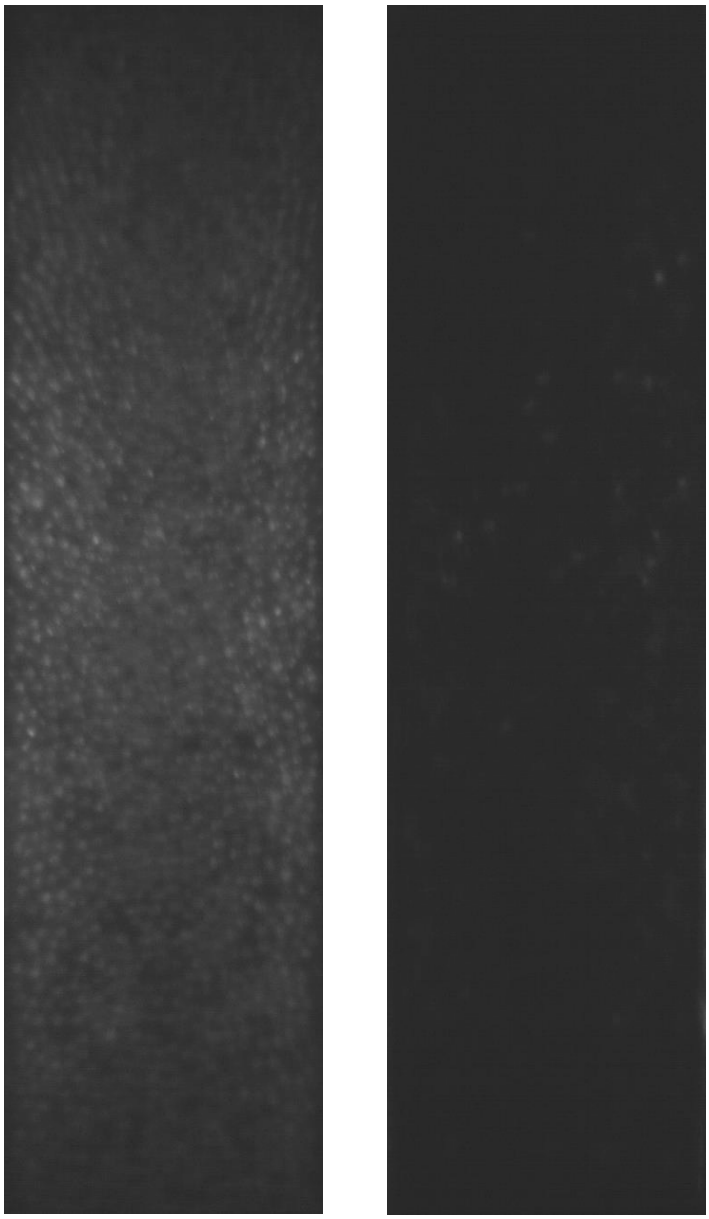

Figure 9: Drill test pictures taken with 1000 FPS and the drill running at 100 RPM. On the left with only white particles and on the right with 90 weight% black particles and 10 weight% white particles.

3.2 Comparison with PEPT

A second method to test the accuracy of the BPIV technique and to find the best settings for this technique was to try and reproduce the experimental results of Lavermans [9]. Oldeman [12] already did a similar test with the setup that was being used in this project. His attempt to reproduce the same results was unsuccessful. He performed several experiments and he compared the obtained results with PEPT data that was presented by Laverman [9]. He found that axial velocity of particles are very close to zero in some cases and they do not follow the similar trend as the PEPT results. To prevent obtaining the same results, a couple of steps were taken.

First the software settings were checked. For processing the data, DaVis is used to create the Microsoft Visual C files. These files contain all the calculated parameters by DaVis software, which can be read with a MATLAB script to get a final average test results. The MATLAB script has been checked and no errors were found. The best settings for DaVis with reasonable processing time has been found through trial and error. It should be noted that the rotating drill test images were used for this purpose. As the analytical results for these tests were available, we could find the best settings. The results can be found in table 8, the settings that are not mentioned in these table are kept at default conditions.

The software was functioning properly and therefore the next step was to check the hardware. It was found that during fluidization, especially at relatively low superficial velocities, the bubbles were only appearing on one side of the fluidized bed. This affected the fluidization of the bed drastically. To be able to check if the distributor was still working properly the setup had to be opened. After opening it was obvious that the gasket was not properly installed. After properly reinstalling the gasket, the fluidization of the bed was checked and a uniform gas distribution was observed.

The particles that Oldeman [12] used were transparent glass particles. For a good image capturing at high amount of FPS, the amount of reflecting light should be maximized. Therefore the shining white particles, 45015-427-WI, from the Sigmund-Lindner Company were used instead. The difference between the used particles can be seen in figure 10. Where picture (a) and (b) are made by Oldeman [12] with an exposure time of 500 and 986 μs, respectively. Picture (c) is made during this project with the white particles and an exposure time of 996 μs.

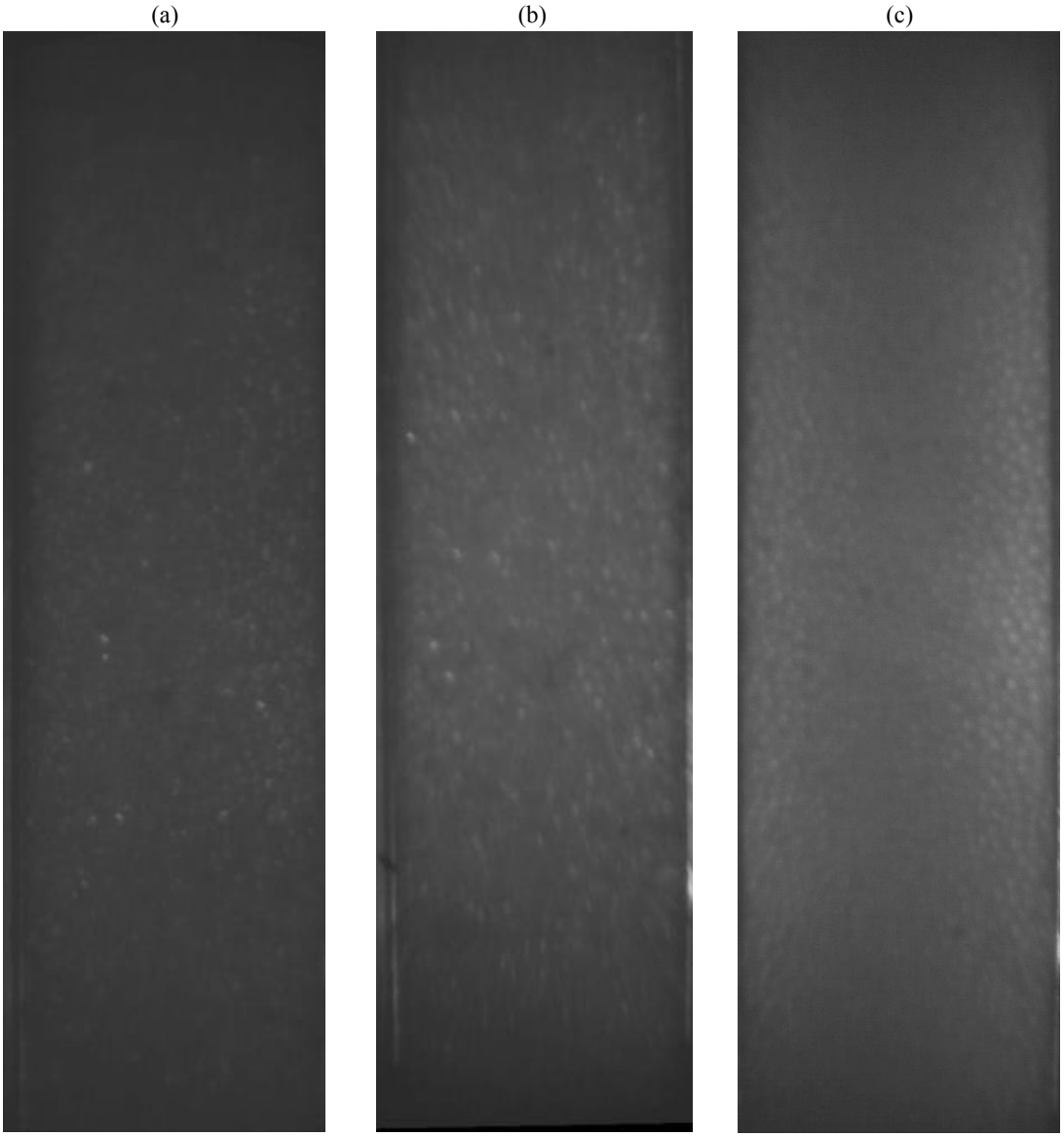

Figure 10: A comparison between the pictures (a)(b) Oldeman [12] made with transparent particles and the picture (c) made in this project with white particles.

Table 8: Used settings for DaVis.

DaVis settings	Value
Stretch arbitrary > Parameter	
Stretch arbitrary X-factor	0.5
Stretch arbitrary Y-factor	0.5
PIV time-series > Vector calculation parameter	
Multi-pass (decreasing size) initial step:	
Windows size	128 x 128
Interrogation window weighting	Round 1:1
Overlap	50
Passes	1
Multi-pass (decreasing size) final step:	
Windows size	48 x 48
Interrogation window weighting	Round 1:1
Overlap	75
Passes	2

Table 9: Most important settings in GenICam Explorer v.5.3.400.

Settings	Value
Image format control # Width	1408
Image format control # Height	428
Image format control # Offset X	384
Image format control # Offset Y	684 (depends on position of the camera)
Acquisition Frame Rate	1000
Exposure Time	996

After repairing the gasket, the fluidized bed showed a uniform gas distribution the experiments could be continued. The goal was to determine the average vertical velocities at different radial positions in the fluidized bed. This was done by placing the ocular inside the fluidized bed at various angles. The middle of the ocular was at a height of 0.21 m from the gas distributor, where only the information of the images between a height of 0.20 m and 0.22 m was used for the final analysis. Laverman [9] also conducted his experiments at the same height.

The BPIV measurements were done at 10 different radial positions. Thus, the borescope was rotated in a way that was possible to capture solid movement at 10 equidistance radial positions. The different measurement positions with their corresponding angles and distance from center can be found in table 10and a schematic representation of these angles can be found in figure 11. When the ocular was pointed to the center of the bed it had an angle of 0° and an angle of 180° when pointed to the wall of the fluidized bed.
To determine the average vertical velocities at different radial positions the experiments were performed at atmospheric pressure, the superficial velocities were calculated with empirical correlation that is presented by Wen and Yu [3]. Results of the experiments can be found in table 23.

Table 10: Different positions of the ocular, with the angle of the ocular and the distance from the center.

Position	Angle [°]	Distance from center [mm]
1	0	17
2	21	30
3	35	43
4	47	56
5	60	69
6	74	82
7	89	95
8	107	108
9	129	121
10	180	134

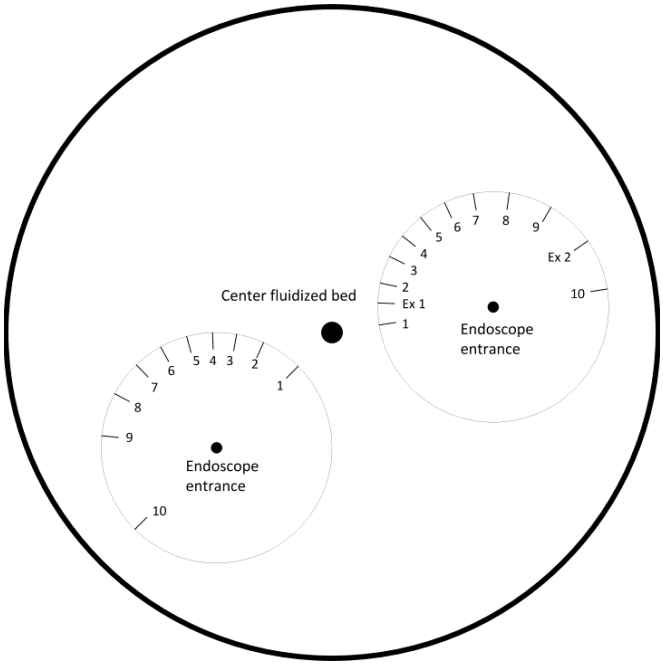

Figure 11: Fluidized bed as seen from the top with the entrance of the borescope and the different angles that are used for it.

For every position two different camera settings were chosen to find the best camera settings. The first camera setting took pictures with 500 frames per second (FPS) and had an exposure time of 1,992 µs, the second camera setting was set to 1000 FPS with an exposure time of 992 µs. A comparison of the different image intensity can be found in figure 12. After cutting the parts that did not display any information of the particles, pictures with a resolution of 1236*361 pixels were obtained. These pictures displayed the particles too big for good processing with DaVis, so it was necessary to resize them to half of their original size in each direction. This was configured to be done by DaVis. All the DaVis settings can be found in table 8. Where the most important settings of the camera can be found in table 9.

Picture (a) in figure 12 has an exposure time of 992 µs and the pictures b and c have an exposure time of 1992 µs, therefore the intensity of these images is slightly higher. Picture c is taken 2 ms later than picture (b). Also an air bubble is visible in these two pictures, which causes the

particles in the top to "rain" down and the particles in the bottom to move up. Picture d is the result of processing of picture (b) and (c) with DaVis.

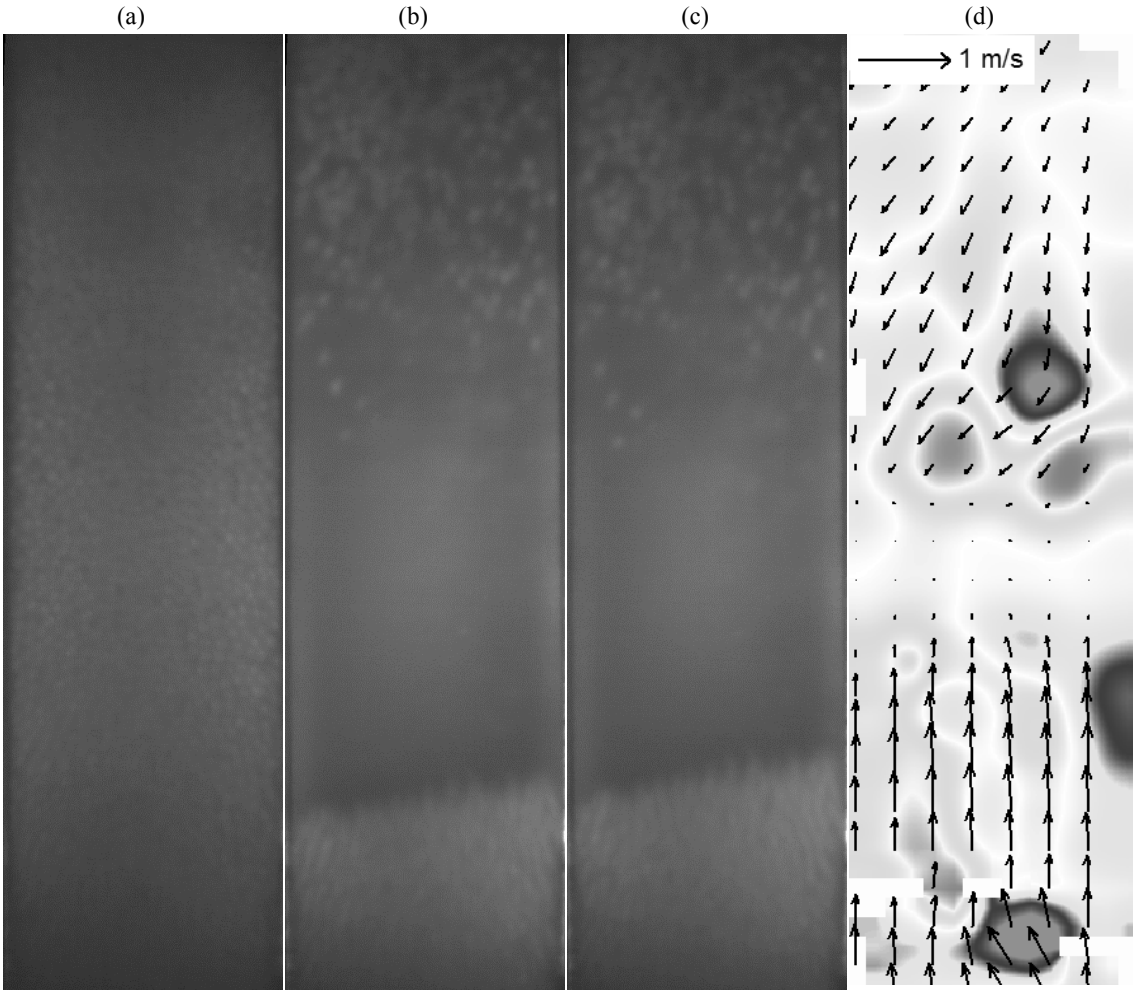

Figure 12: All four pictures are taken at position 9 at atmospheric conditions with a superficial fluidization of 0.29 m/s. Picture (a) is taken with 1000 FPS and an exposure time of 992 µs. Pictures (b) and (c) are taken with 500 FPS and an exposure time of 1992 µs. Picture d is the result after processing the pictures (b) and (c) with Davis.

After performing all the experiments, the pictures were processed with Davis. That leaded to 9,999 Microsoft Visual C files for every experiment with 10,000 pictures. These Microsoft Visual C files display the velocities of every interrogation area between every image, as can be seen in the right side of figure 12. The final results of this test can be found in figure 13 and figure 14 where the PEPT results by Laverman [9] and BPIV results by Oldeman [12] can be found too.

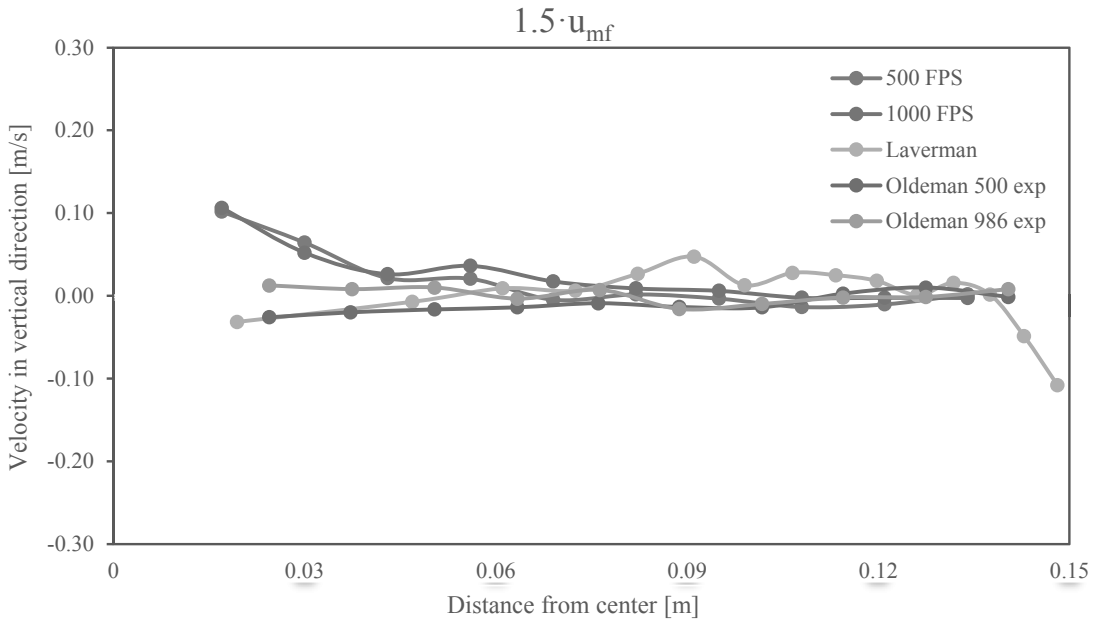

Figure 13: Test result of the time-average velocity in vertical direction done with 500 and 1000 FPS with a superficial velocity of 0.28 m/s, compared with Lavermans [9] and Oldemans [12] results.

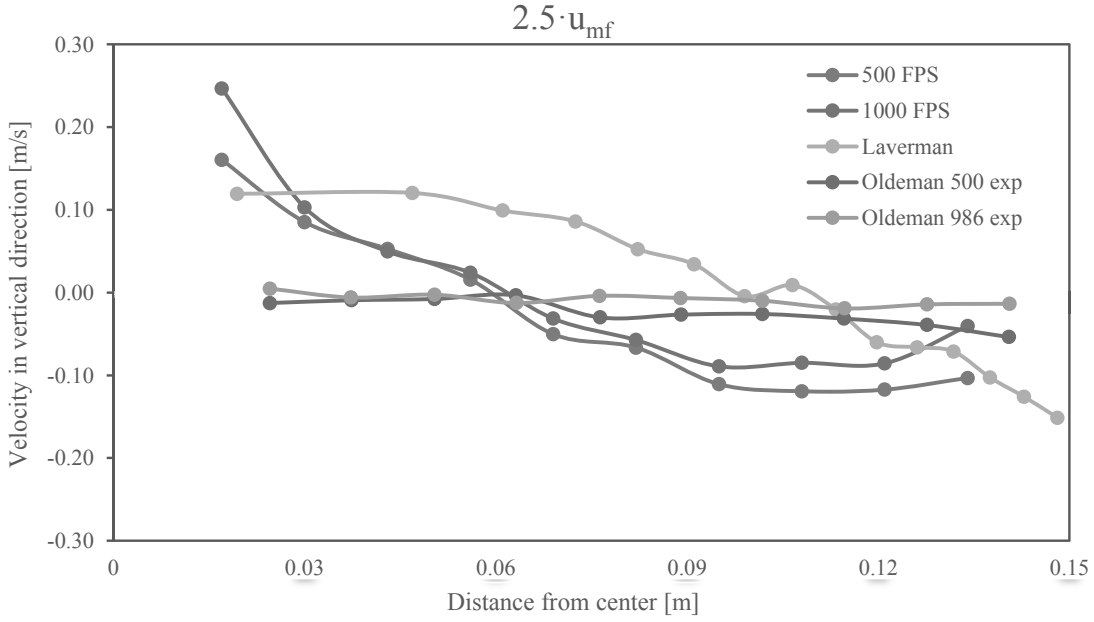

Figure 14: Test result of the time-average velocity in vertical direction done with 500 and 1000 FPS with a superficial velocity of 0.48 m/s, compared with Lavermans [9] and Oldemans [12] results.

3.2.1 Discussion

It should be noted that Laverman [9] did experiments in a similar 3D fluidized bed but with positron emission particle tracking (PEPT). PEPT is a non-intrusive technique where a radioactive labeled particle is tracked while moving through a measuring vessel. When two measurements within a short time interval are known, the velocity of the particle can be calculated. This calculation is done with the assumption that particles are moving in a straight

line within this time interval. A schematic representation of a PEPT setup is shown in figure 15.

The data in this project is directly comparable with Laverman [9]. Where Laverman [9] correctly measured the particle velocity, while the experiments in this project do not account for the gas fraction. When a bubble is seen by DaVis, it sees a velocity of zero, but this "false" velocity is taken into account in the calculation of average velocity. Also the amount of solid fraction is not taking into account. If there are particles in the measured cells, DaVis will just give the average velocity and does not take into account the number of particles.

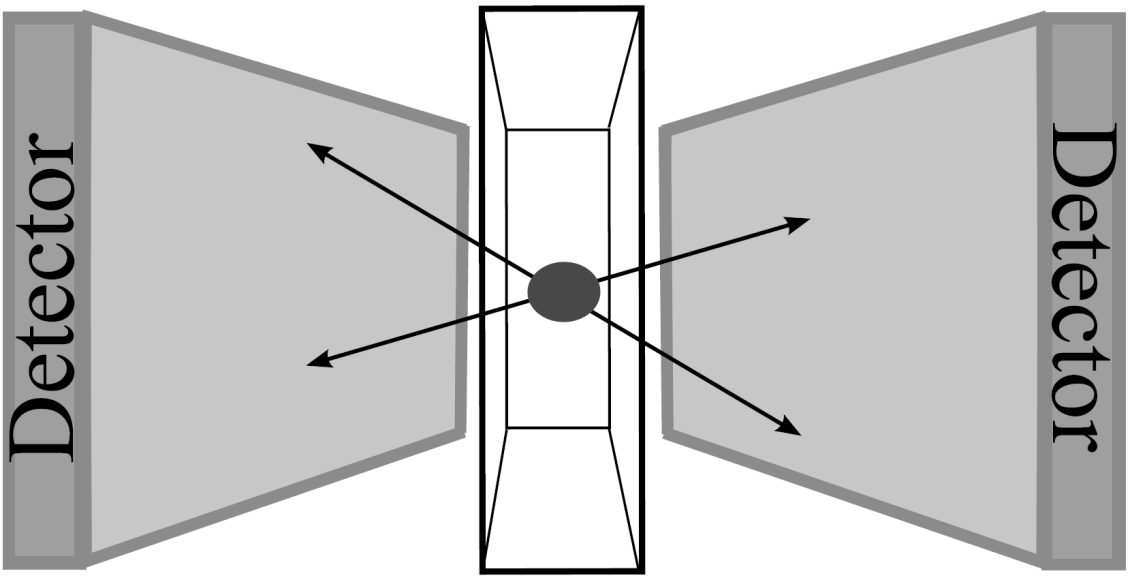

Figure 15: Schematic representation of a PEPT setup [9].

Recently, Tebianian et al. [10] did a comparison of measuring the particle velocities with different techniques like the borescope, which is similar to the borescope that is used in this project, and the PEPT, that is also used by Laverman [9]. Tebianian et al. [10] found significant differences in the results when using the different measurement techniques. Figure 16 presents a selection of their results in a 0.133 m diameter fluidized bed with a static bed height of 0.82 m. In the end, they concluded that the PEPT measurements should be the most accurate one as it is non-intrusive and the tracer particle is very similar to the fluidizing particles. Tebianian et al. [10] made 11 graphs at different heights and various superficial gas velocities in total, in 11 graphs, Tebianian et al. [10] plotted a total of 55 data points. As in the steady state condition, the amount of particles going up should be the same as the amount of particles going down, probably there is a systematic error in their PEPT measurements because 54 of the 55 data points are negative and thus have more particles moving down than going up. Consequently, their conclusion should be revised and checked even though that is expected to get the best results with PEPT technique.

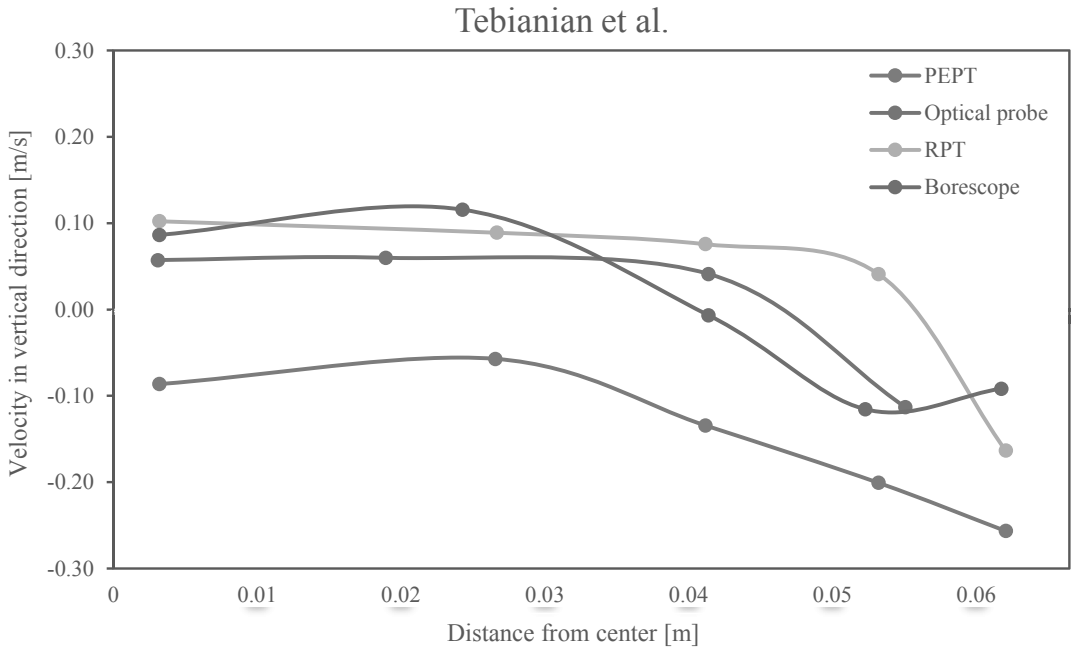

Figure 16: Tebianian et al. [10] result of different measurement techniques. This results are at 0.24 m above the distributor and at superficial gas velocity of 0.40 m/s.

3.2.2 Conclusion

The results found in this experiment are more in line with literature and appear to be a more logical than the results from Oldemans [12] , especially at $u=2.5 \cdot u_{mf}$. Therefore it can now be concluded that the fluidized bed is working properly again. Similar trends in this experiment and Lavermans [9] results were observed. In both experiments the particles near the center of the fluidized bed go up and they tend to go down far from the center. However there is a difference between the absolute values found in both experiments. Tebianian et al. [10] showed that these results could be due to the different nature of measurement techniques.

It is also noticed that, the difference between the results of 500 and 1000 FPS measurements are very small and both FPS setting captures images with a high enough light intensity to be processed by DaVis. Therefore, it is suggested to use 1000 FPS settings for fluidization at high velocities and 500 FPS settings can be used for fluidization at velocities close to minimum fluidization condition.

3.3 Sensitivity analysis

To minimize the processing time, the amount of data should be as little as possible. Every test creates 10,000 pictures, which depending on the camera settings, 500 or 1000 FPS, gives a measuring time of 10 or 20 seconds. The measurement time should be as short as possible to decrease the processing time, but should be long enough to get a representative result. Therefore a sensitivity test to the measurement time has been performed and the results are presented and discussed in this section.

In table 11 and table 12 the results of the sensitivity test are given, with the results for the 10 different positions. These results are displayed in figure 17 and figure 18. The sensitivity test

was executed with two different settings. The first test was done with 500 FPS and at $1.5 \cdot u_{mf}$ and the second test was done at 1000 FPS and at $2.5 \cdot u_{mf}$.

Table 11: Sensitivity test results with $1.5 \cdot u_{mf}$ and 500 FPS.

Position	2.5 [s]	5 [s]	10 [s]	15 [s]	20 [s]
1	0.140	0.136	0.109	0.101	0.102
2	0.080	0.074	0.073	0.065	0.064
3	0.021	0.019	0.026	0.024	0.022
4	0.017	0.025	0.018	0.014	0.021
5	-0.009	-0.007	-0.006	-0.008	-0.005
6	0.010	0.001	0.000	-0.002	0.002
7	0.006	0.001	0.001	-0.002	-0.003
8	-0.021	-0.013	-0.014	-0.014	-0.013
9	-0.016	-0.008	-0.006	-0.009	-0.010
10	0.016	0.010	0.004	0.000	0.002

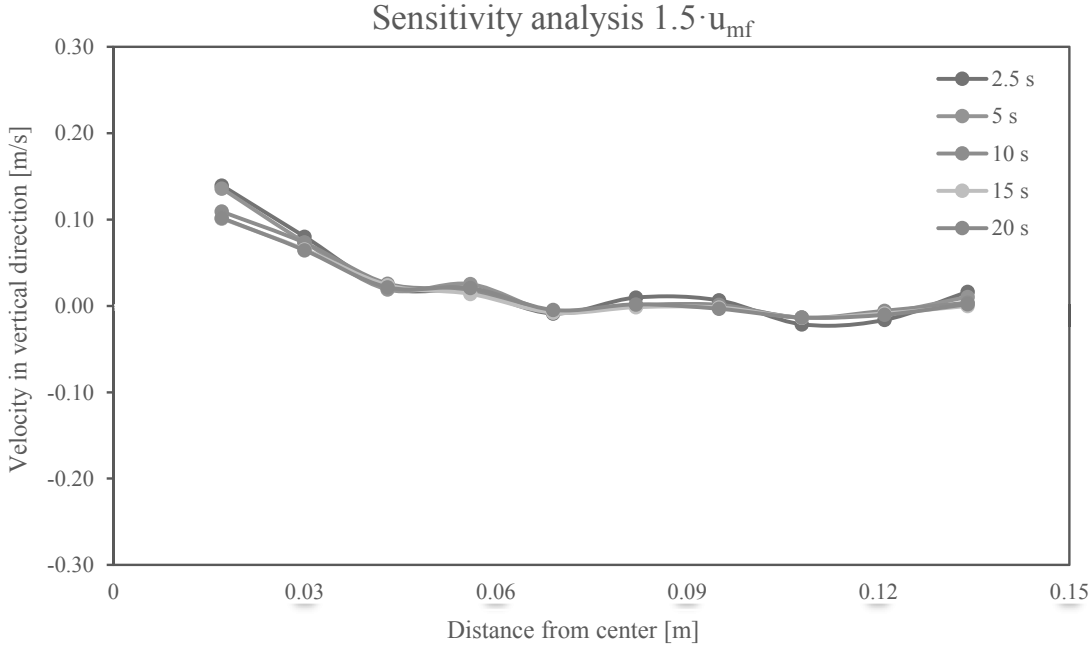

Figure 17: Sensitivity of the results to the measurement time at $1.5 \cdot u_{mf}$ and 500 FPS.

Table 12: Sensitivity of the results to the measurement time at $2.5 \cdot u_{mf}$ and 1000 FPS.

Position	1.25 [s]	2.5 [s]	5 [s]	7.5 [s]	10 [s]
1	0.171	0.215	0.243	0.246	0.247
2	0.138	0.110	0.080	0.090	0.103
3	0.034	0.039	0.035	0.046	0.050
4	-0.010	-0.012	0.015	0.014	0.024
5	-0.039	-0.016	-0.031	-0.040	-0.031
6	-0.052	-0.045	-0.051	-0.055	-0.057
7	-0.071	-0.099	-0.090	-0.094	-0.089
8	-0.087	-0.125	-0.086	-0.081	-0.085
9	-0.084	-0.086	-0.085	-0.089	-0.085
10	-0.037	-0.034	-0.042	-0.047	-0.040

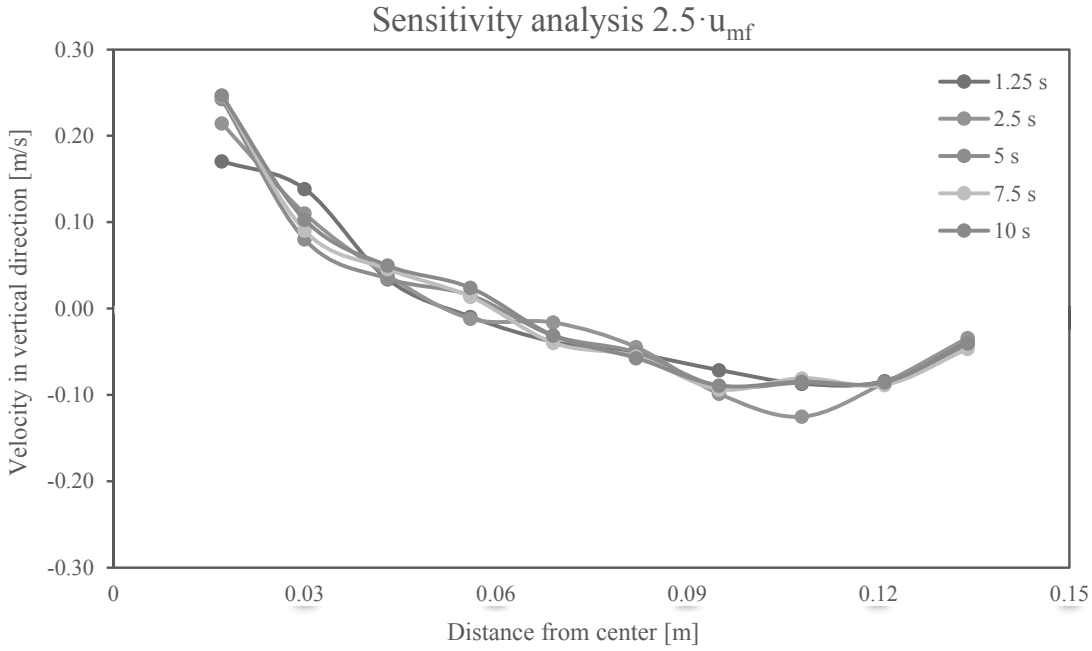

Figure 18: Sensitivity of the results to the measurement time at $2.5 \cdot u_{mf}$ and 1000 FPS.

3.3.1 Conclusion

From the figures it can be observed that there is no significant change after 75% of the measuring time. So, to minimize the processing time it was decided to reduce the measurement time to 7.5 s and 15 s for experiments for 1000 FPS and 500 FPS settings respectively.

3.4 Temporal histogram method

After validating the BPIV technique, it is decided to check the possibility of improving BPIV accuracy. For this reason, temporal histogram method (THM) was applied to all the images as a preprocessor. This method has been developed for removing light non-homogeneities [15]. One of the benefits of this method, is that the bubbles can be clearly seen in the pictures, as can be seen in figure 19.

In figure 20 a comparison is made between the Comparison with PEPT test with and without applying THM on images. The results showed similar trends and similar order of magnitude. Pre-processing of the pictures with the THM adds another hour of processing time to every data point that contains 7500 frames. Thus, THM was not used for this project afterwards.

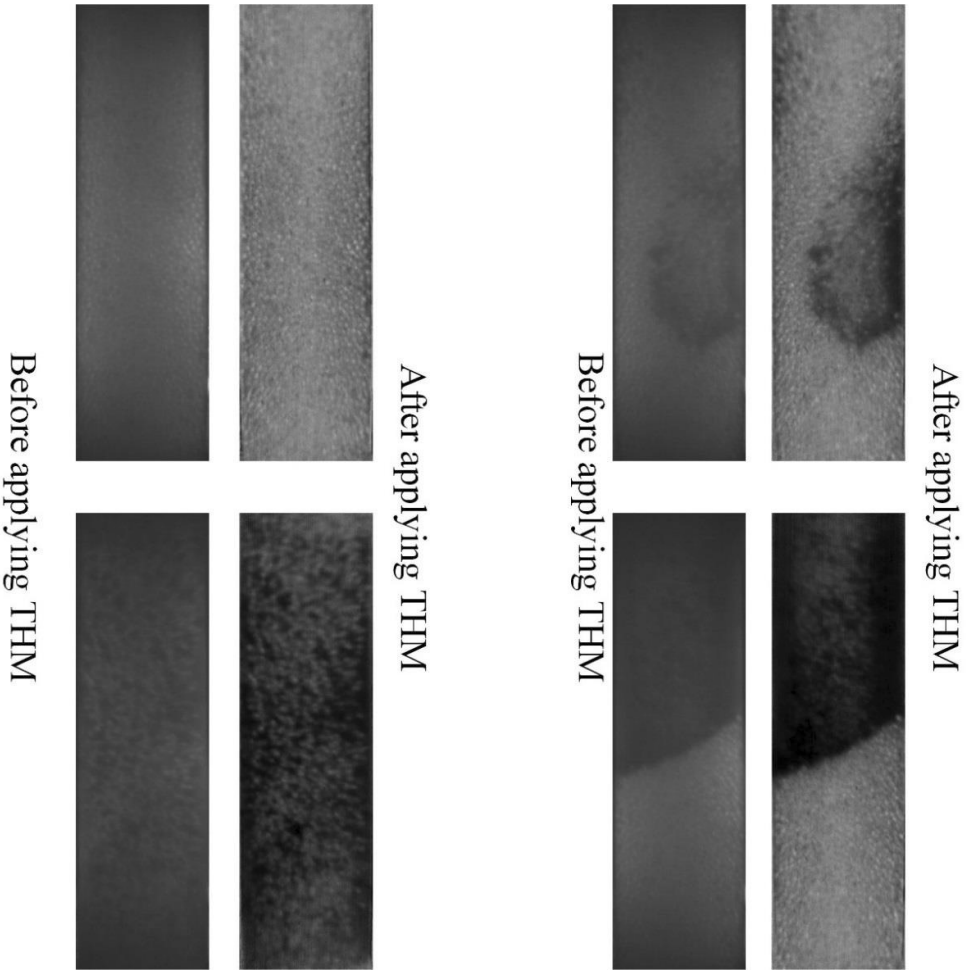

Figure 19: Borescopic images before and after applying THM technique on them.

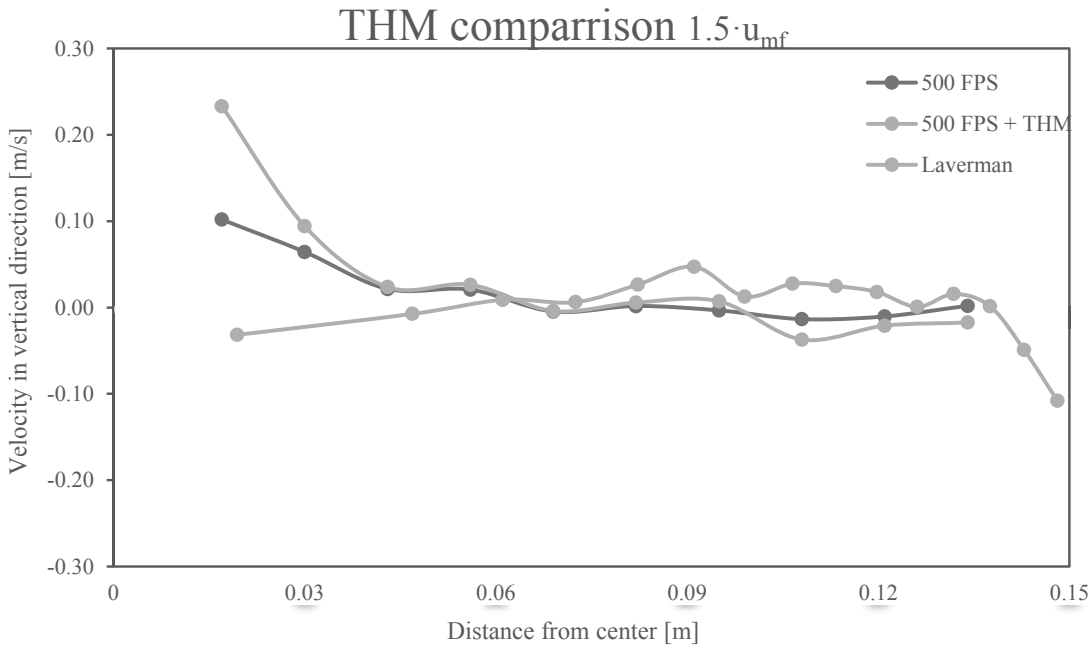

Figure 20: Comparison of PEPT results with BPIV results with and without applying THM on the images.

3.5 Uniformity of gas distribution and position sensitivity analysis

The 3D fluidized bed should run in a symmetrical way, where the velocity of the particles and the amount of bubbles should be equal to each other at every equal distance from the center of the fluidized bed within a long enough period of time. To test if this is true for the performed experiments in this project, several experiments were conducted. In these experiments the top of the fluidized bed was moved 126° in a counter-clockwise manner, when looking from the top of the fluidized bed. Also the camera position was mirrored to go from 360° to 180° instead of 0° to 180°. The camera and ocular positions in the original and new experiments can be found in table 13 and a corresponding picture can be found in figure 11. As the distance between positions 1 and 2 and the distance between positions 9 and 10 are quite large, two additional experimental points were added to the measurement positions. These two points and their corresponding angels are mentioned in table 13 as ‘Extra 1’ and ‘Extra 2’.

Table 13: Different positions of the ocular, with the angle of the ocular and the distance from the center.

Position	Angle [°]	Distance from center [mm]
1	360	17
Extra 1	349	21
2	339	30
3	325	43
4	313	56
5	300	69
6	286	82
7	271	95
8	253	108
9	231	121
Extra 2	206	131
10	180	134

It should be added that the new experiments were performed with a gas velocity of $2.5 \cdot u_{mf}$ and a 1000 FPS image capturing frequency.

3.5.1 Results

The results of this test can be seen in table 14 and figure 21. The test results were quite similar when comparing with PEPT results. Although the results of position 1 and 4 slightly changed after changing the borescope position. Therefore these positions were repeated a couple of times as can be seen in table 15, table 16 and figure 21.

Table 14: Results of sensitivity analysis at $2.5 \cdot u_{mf}$.

Distance from center [m]	Velocity [m/s]
0.017	0.166
0.021	0.128
0.030	0.123
0.043	0.130
0.056	0.005
0.069	-0.005
0.082	-0.040
0.095	-0.095
0.108	-0.060
0.121	-0.109
0.130	-0.133
0.134	-0.098

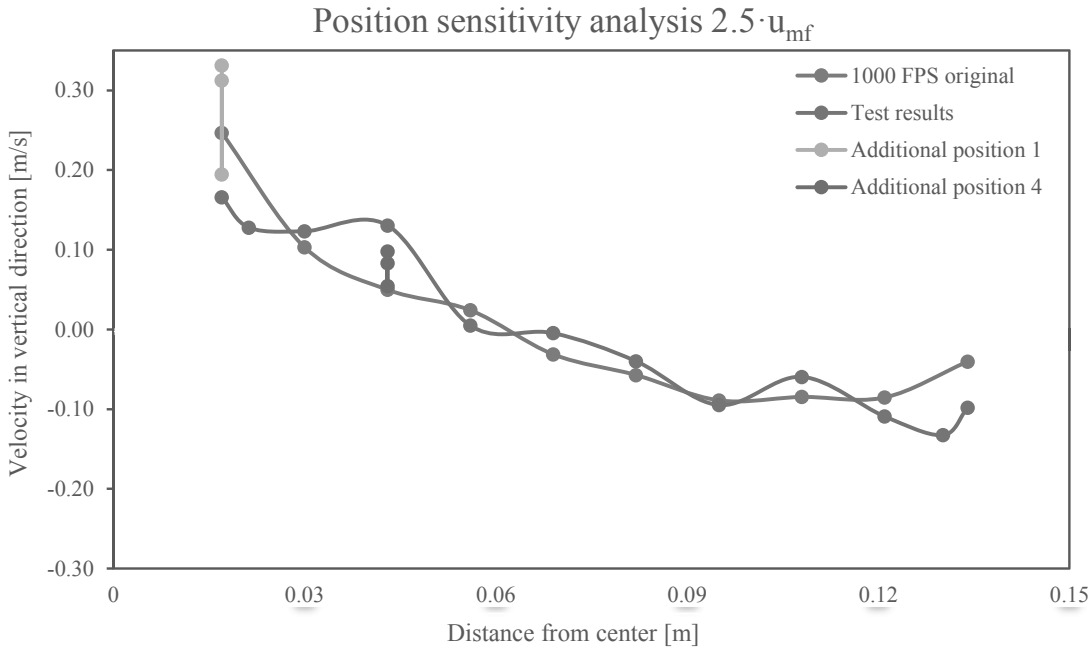

Figure 21: Particle velocity compared at the original position and the new position with $u_g = 2.5 \cdot u_{mf}$.

Table 15: Results of sensitivity analysis at $2.5 \cdot u_{mf}$, additional point 1.

Distance from center [m]	Velocity [m/s]
0.017	0.312
0.017	0.194
0.017	0.331

Table 16: Results of sensitivity analysis at $2.5 \cdot u_{mf}$, additional point 2.

Distance from center [m]	Velocity [m/s]
0.043	0.098
0.043	0.054
0.043	0.083

3.5.2 Conclusion

The BPIV results did not change considerably after changing the position of the borescope. Therefore, it can be concluded that the distributor and the fluidized bed are working properly and in a symmetrical way. Also the two additional points showed values that quite comparable with their neighboring points. Thus, these two additional points are not investigated in the final experiments in the pressurized fluidized bed.

3.6 Effect of illumination power

In this section, the effect of illumination power is presented and discussed. For this purpose, the time-average velocity profile in the radial direction was obtained while only half of the highest possible illumination power was applied. The results can be seen in table 17 and figure

22. As can be seen, the solid velocity decreases significantly with decreasing the light illumination power. Figure 23 presents two images with applying different amount of light source. This figure clearly shows that the intensity of the left picture is higher than the image intensity in the right image. As the image intensity drops considerably with decreasing the illumination power, tracking of particles and determining of their velocities becomes very difficult. Thus, most of the velocities will be very close to zero and the final average velocity will be very close to zero too.

Table 17: Results of effect of illumination power at $2.5 \cdot u_{mf}$.

Distance from center [m]	Velocity [m/s]
0.017	-0.0071
0.021	0.0009
0.030	-0.0047
0.043	0.0002
0.056	0.0014
0.069	0.0009
0.082	0.0029
0.095	0.0012
0.108	0.0014
0.121	0.0015
0.130	0.0018
0.134	0.0041

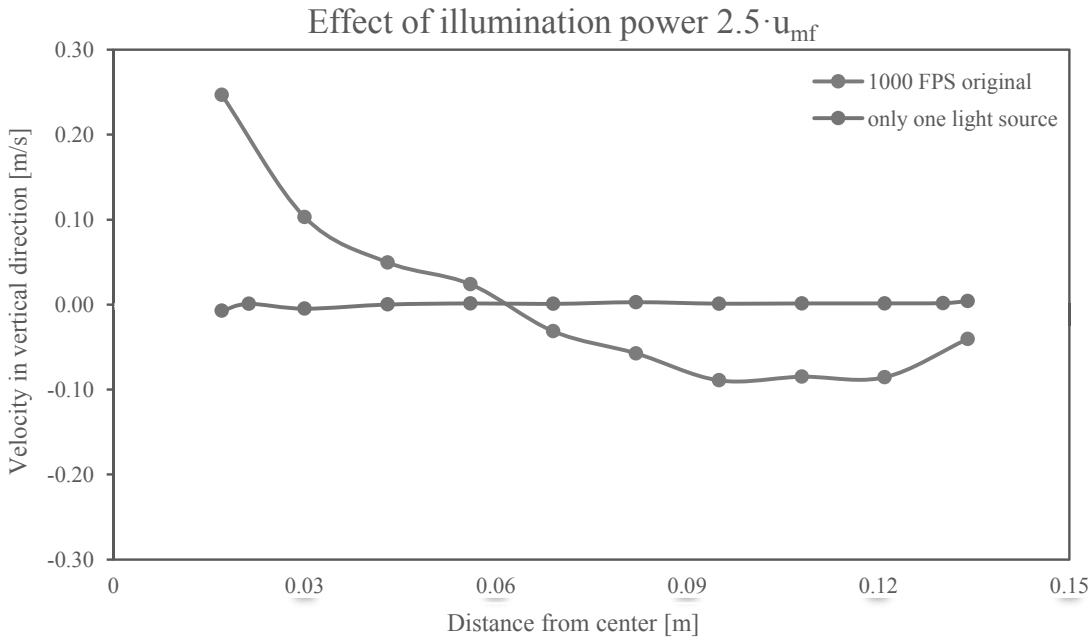

Figure 22: Effect of illumination power on the BPIV results with $u_g = 2.5 \cdot u_{mf}$.

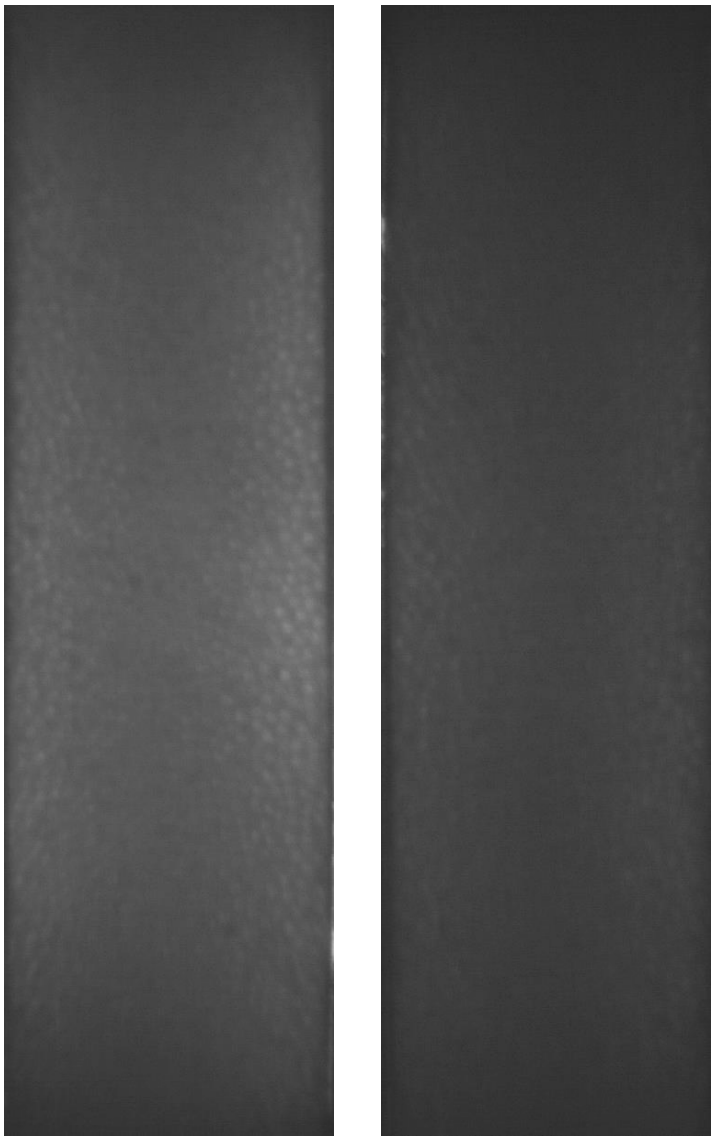

Figure 23: On the left an image with applying the highest possible illumination power and on the right an image with applying half of the highest possible illumination power.

3.7 Effect of particles light reflectivity

In this section, the effect of particle's light reflectivity is presented and discussed. The results of this test can be found in table 18 and figure 24. It is observed that with decreasing the particle's light reflectivity, the time-average solid velocity decreases. When the light reflectivity of particles decreases, their detection becomes harder. Consequently, there will be some zero velocities in the processing results even though the particles are moving. Thus, the average solid velocity decreases when the particle's light reflectivity decreases.

Table 18: Results of effect of illumination power at $2.5 \cdot u_{mf}$.

Distance from center [m]	Velocity [m/s]
0.017	0.062
0.017	0.092
0.017	0.077
0.017	0.064
0.017	0.078
0.021	0.085
0.030	0.003
0.043	0.006
0.056	-0.036
0.069	-0.070
0.082	-0.096
0.095	-0.093
0.108	-0.105
0.121	-0.122
0.130	-0.083
0.134	-0.063

Table 19: Results of effect of illumination power at $2.5 \cdot u_{mf}$, for additional points.

Distance from center [m]	Velocity [m/s]
0.017	0.069
0.017	0.052
0.017	0.051
0.017	0.055

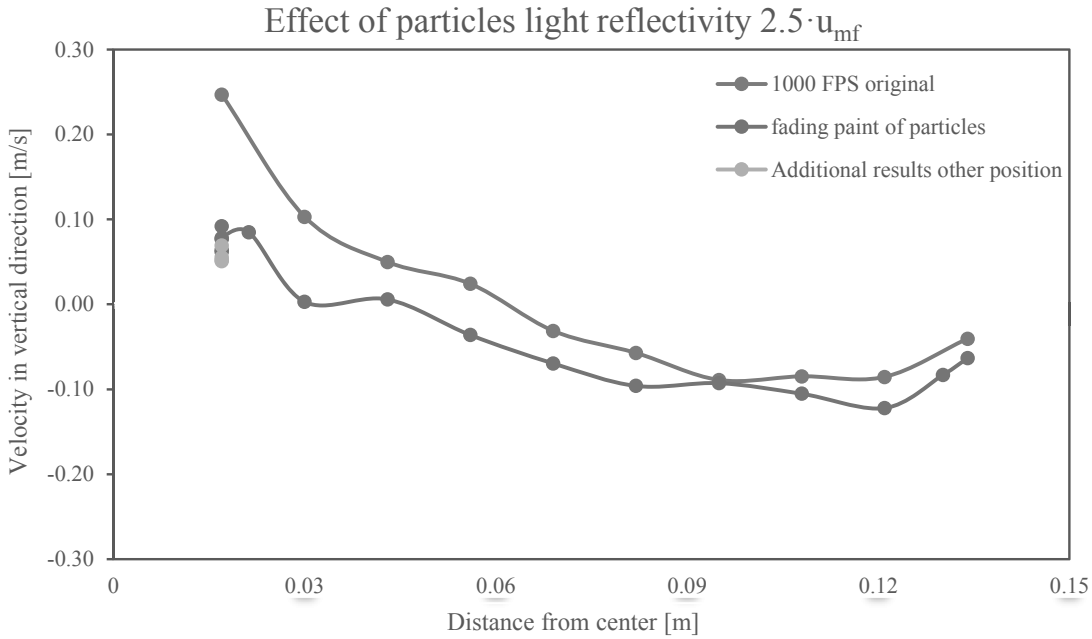

Figure 24: Effect of particles light reflectivity on the BPIV results at $u_0=2.5\cdot u_{mf}$.

As the particles that has been used in this project lose their color with time, they may give some of their colors to the observation window (ocular). Figure 25 shows an image of ocular before and after using in the fluidized bed. This may cause some errors in the images.

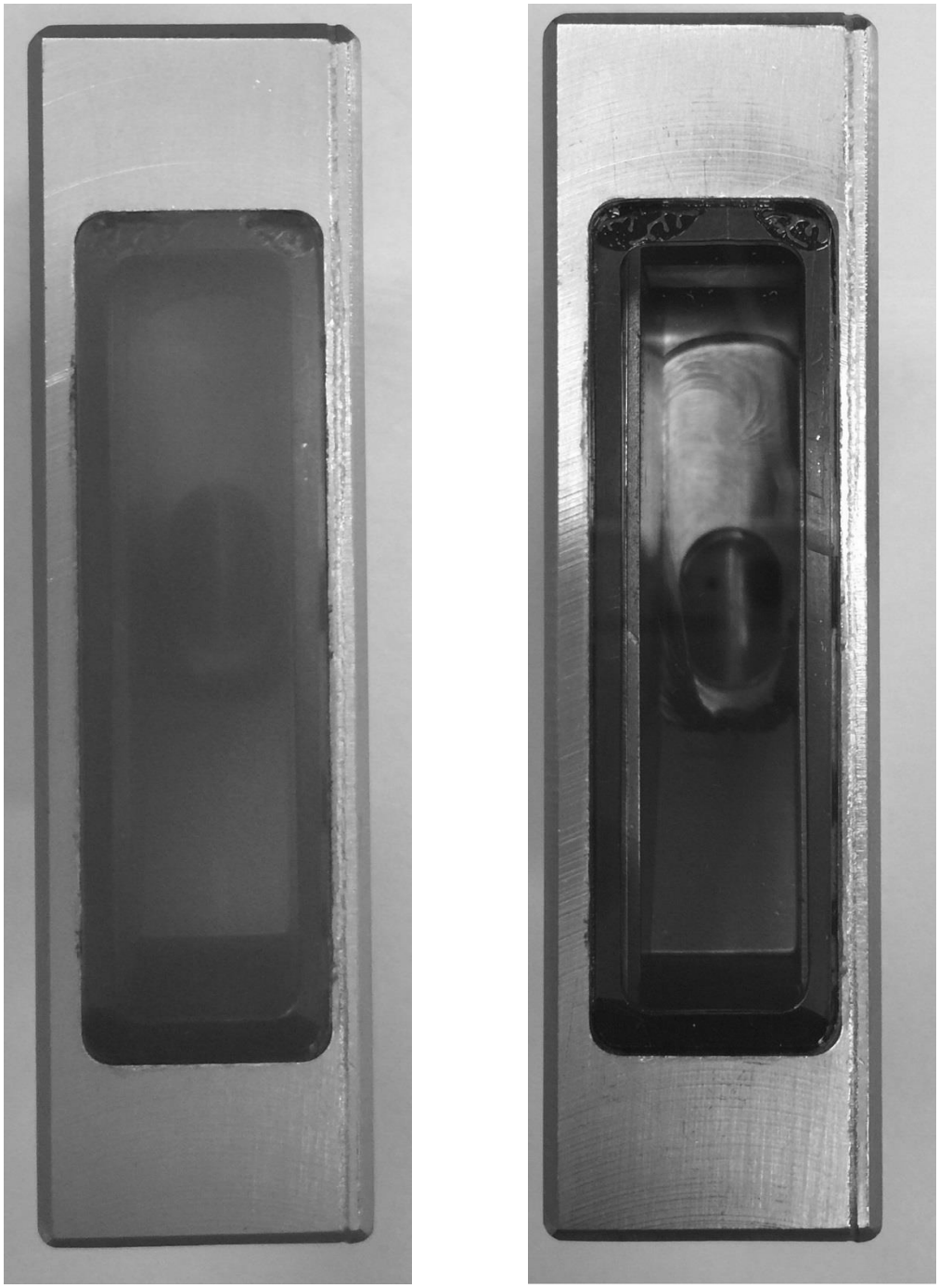

Figure 25: The ocular. Left: is after running experiments. Right: after cleaning.

In figure 26 the images that the ocular captured can be seen. Pictures (a) and (b) are taken when ocular is in the fluidized bed, where (a) is at the beginning of the experiments and (b) is after a lot of experiments are done and the particles lost some of their colors and the ocular became dirty. In picture (c) and (d), the ocular is cleaned and is put in non-moving particles. Where (c) is a picture with new particles and (d) with the particles that were already used for a lot of experiments.

Thus, it is necessary to use the fluidized bed as less as possible, clean the ocular frequently or using particles which does not lose their pigments.

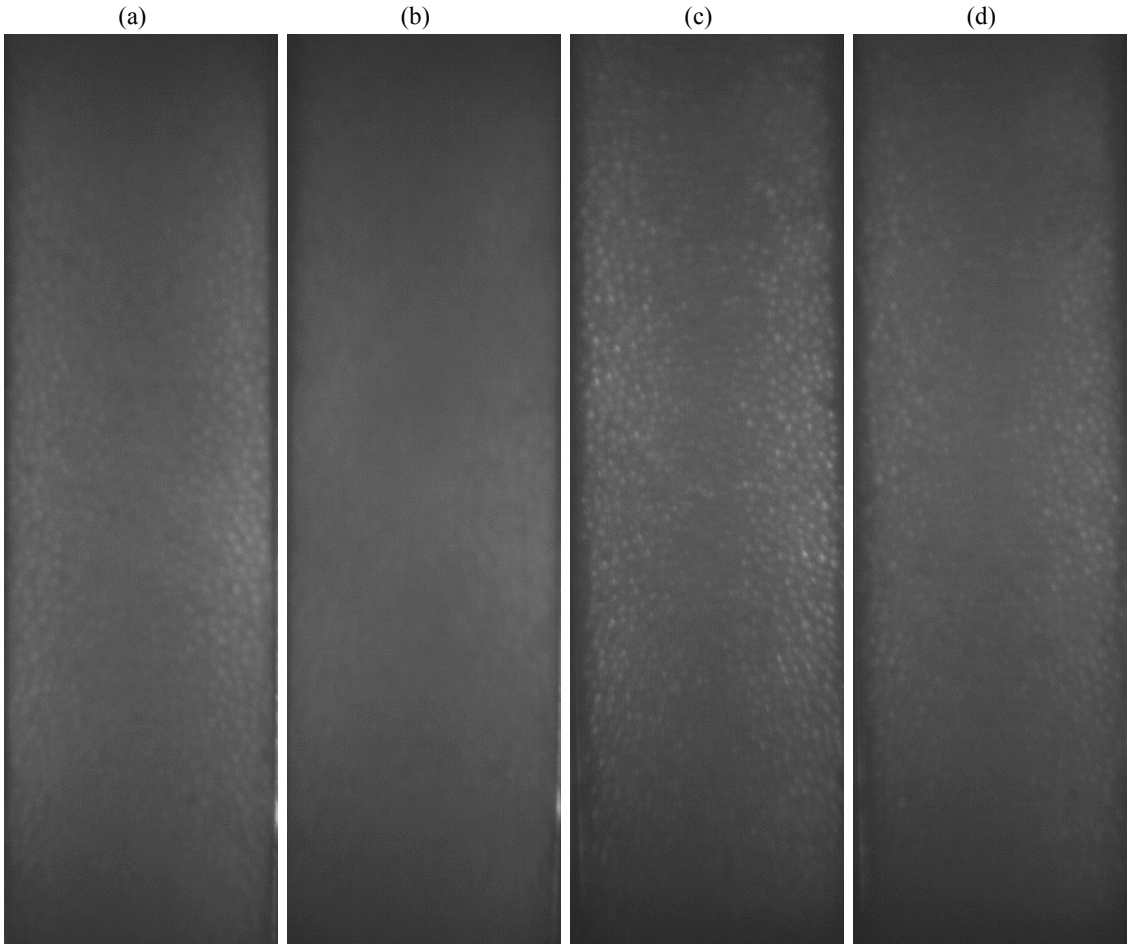

Figure 26: Different images qualities at different conditions of the paint and fouling of the ocular.

3.8 Speeding up the process

Due to the high amount or processing time that is required to compute every data point. There has also been a small research in optimizing the data processing workflow. A lot of time could be saved by using the "batch processing" option that is built in DaVis. Here a maximum of 10 data points could be done in one batch, which could run overnight. Also the MATLAB scripts could be automated to a certain extent. The processing time that is required for the computer to process the data can be found in table 20. The specifications of the computer that is used for processing can be found in table 21. Also a normal "office" computer was used for processing this data, but it was found to be too slow for it. If the computer time has to be faster it is advisable to use an SSD as storage drive.

Table 20: Time [min] needed for every step.

Processing of 7500 pictures, resulting in one data point	Time [min]
Setting ocular in correct position	10
Pressuring fluidized bed from 1 to 16 bar	300
Depressurizing fluidized bed by 1 bar	2
Taking pictures with camera	5
Saving the pictures from the camera	2
Rotating and cutting the pictures with MATLAB	6
Importing and scaling pictures in Davis	12
Process pictures with Davis	70
Saving Microsoft Visual C files	1
Reading Microsoft Visual C files for average velocity	5
Total (without considering the time for pressurizing of the bed)	111

Table 21: Specifications of the computer.

Computer specifications	
Operation system	Windows 7 Enterprise 64-bit SP1
Processor	Intel Core i5 4670 @ 3.40GHz
RAM (Random-access memory)	2*8 GB Dual-Channel DDR3 (11-11-11-28)
Motherboard	Hewlett-Packard 18E4
Graphics	Intel HD Graphics 4600
OS drive	238GB ATA SAMSUNG MZ7PD256 SCSI Disk Device (SSD)
Data drive	3725GB Western Digital WD My Book 1230 USB Device (USB (SATA))

3.9 Intrusiveness of BPIV technique

The intrusiveness of the ocular and the borescope is hard to quantify. The horizontal area of the ocular is (7.0 cm · 2.2 cm=) 15.4 cm^2. The horizontal area of the fluidized bed is (1/4 · 30.6^2 cm=) 735.2 cm^2. This causes the area of the fluidized bed at the height of the camera to shrink by 2.1% and get a superficial gas velocity that is 2.1% higher. Which leads to a new equilibrium state at the height the camera is inserted.

The intrusiveness of the technique can be observed clearly when the fluidized bed operates at velocities close to the minimum fluidization condition. In these conditions, all the bubbles escape to the surface at the spot where the ocular is placed. If the fluidized bed operates at much higher velocities than minimum fluidization velocity, this phenomena is less pronounced and the bubbles are formed quite uniformly at the dense zone-freeboard interface.

3.10 Errors in the measurement

During the experiments several flaws in the measurements were observed. In this paragraph these flaws will be explained.

The first flaw is that the saving of the captured pictures starts at a random point. When the pictures are saved, the first named picture is not the first one taken. But the camera starts taking

the first picture at a random point and continues from that point. This causes an error in the calculation with DaVis that starts processing from the first named picture. The problem is solved by manually changing the name of the first picture when less than 200 pictures were taken. With a higher amount of pictures, this problem becomes negligible.
The second flaw is that DaVis cannot see the difference between the amounts of particles in a cell. When there is a bubble in that cell, DaVis recognize this as a velocity of zero and this velocity will add up to the average particle velocity, when in reality, there is nothing to add up. Also the amount of particles in a cell is something DaVis does not take into account. For example when there are 10 particles in a cell or there is only 1 particle in a cell, both cells are taken as 1 data point. This causes a calculation error, which should be considered during checking of the results.
The third flaw is the particles behind a bubble can also be registered by the camera. When a bubble rises in front of the ocular, some of the particles behind the bubble can still be captured by the camera. However this particles are in a different position than where the measurement is taking place. This causes to have a particle velocity of a different place to be measured.
The fourth flaw is that the ocular becomes dirty after a while. This can be clearly seen in figure 25 and the effect of it can be seen in figure 26. This problem can be solved by using particles that do not lose their paint or by minimizing the friction between the particles (i.e. by using the fluidized bed as less as possible).
The fifth flaw is that the stick that is used to connect the ocular and the camera moves a little bit when the fluidized bed is running. This effect is pronounced at a large fluidization velocities. A partly solution for this problem is to mount the stick very tight.
The sixth flaw is the shortcoming of the information in the pictures. The program DaVis compares two pictures and tries to get all the information out of them. The only problem is that DaVis does not know what happened between the pictures and therefore always thinks the particles moved in a straight line. This is however not always the case and in this way the measured velocity is lower than actual velocity. A partly solution is to get an as high as possible FPS, which minimizes the movement of the particles between the pictures.

3.11 Conclusion

The ocular that is part of the used experimental apparatus in this project, has an intrusive effect. It is expected to get more accurate results at higher gas velocities. On the other hand, the PIV technique loses its accuracy if the particles move very fast. In other word, it is expected to get the best results with this technique if the gas velocity and consequently the solid velocity is not very low and not very high. The intrusiveness extent of BPIV is not clear to us and it is very good subject for further future researches.

The best settings for DaVis can be found in table 8. The best camera settings, especially for high superficial gas velocities, are 1000 FPS with an exposure time of 992 μs and a minimum of 7500 frames (=7.5 s).

4 Effect of pressure on fluidization

After successfully validating the BPIV technique and finding the best settings to perform the experiments, pressurized experiments could be conducted in the fluidized bed. In this chapter of the report the fluidized bed is put under pressure and its effect on fluidization have been studied.
The experiments are performed under elevated pressures between 1 to 16 bara. The center of the ocular was placed at a height of 0.21 m above the distributor and the vertical velocity of the particles was measured at that height. Only the party between 0.20 and 0.22 m above the distributor is used for the final analysis.

4.1 Minimum Fluidization Velocity

The minimum fluidization velocity (u_{mf}) needs to be calculated in order to set the fluidization velocity. This calculation is explained in this section. The ideal gas law was used for calculating the gas density (ρ_g)

$$\rho_g = \frac{P \cdot M_g}{R \cdot T} \tag{1}$$

Archimedes number:

$$Ar = \frac{d_p^3 \cdot \rho_g \cdot (\rho_p - \rho_g) \cdot g}{\mu_g^2} \tag{2}$$

The Reynolds minimum fluidization velocity is empirically defined by Wen and Yu in 1966 [3]:

$$\mathrm{Re}_{mf} = \sqrt{33.7^2 + 0.0408 \cdot Ar} - 33.7 \tag{3}$$

Reynolds number:

$$\mathrm{Re} = \frac{\rho_g \cdot d_p \cdot u_g}{\mu_g} \tag{4}$$

By combining equations (1.24) and (1.25), the minimum fluidization velocity can be calculated:

$$u_{mf} = \frac{\mathrm{Re}_{mf} \cdot \mu_g}{\rho_g \cdot d_p} \tag{5}$$

The conditions that are used for calculating the u_{mf} can be found in table 22. The u_{mf} for 1 bara has been calculated first. This u_{mf} has been multiplied by 1.5 and 2.5 to get the desired superficial gas velocities for operating the fluidized bed and using in the TFM for 1 bara pressure. The difference between u_{mf} at 1 bara and $1.5 \cdot u_{mf}$ and $2.5 \cdot u_{mf}$, are 0.095 m/s and 0.286 m/s, respectively. These difference are used to compute the other velocities for operating the

fluidized bed under elevated pressures. It can be seen in figure 27 that these superficial gas velocities are within the blower range.

Table 22: Conditions that are used for u_{mf} calculation .

Setting	Value
Gas constant (R)	8.314 [J/(mol·K)]
Temperature (T)	298 [K]
Molar mass of air (M_{air})	0.02897 [kg/mol]
Density (ρ_p)	2,526 [kg/m^3]
Gravity (g)	9.81 [m/s^2]
Dynamic gas viscosity (u_g)	1.8·10^{-5} [Pa·s]

Table 23: Results of u_{mf} and experimenting velocities.

Pressure [bara]	1	2	4	8	16
u_{mf} [m/s]	0.191	0.178	0.159	0.136	0.111
u_{mf} + 0.095 [m/s]	0.286	0.273	0.254	0.231	0.207
u_{mf} + 0.286 [m/s]	0.477	0.464	0.445	0.422	0.397

Table 24: RPM set of the blower to get the desired velocity.

Pressure [bara]	1 (= atm)	2	4	8	16
u_{mf} + 0.095 [m/s]	1820	1570	1360	1200	1060
u_{mf} + 0.286 [m/s]	2980	2580	2370	2160	2030

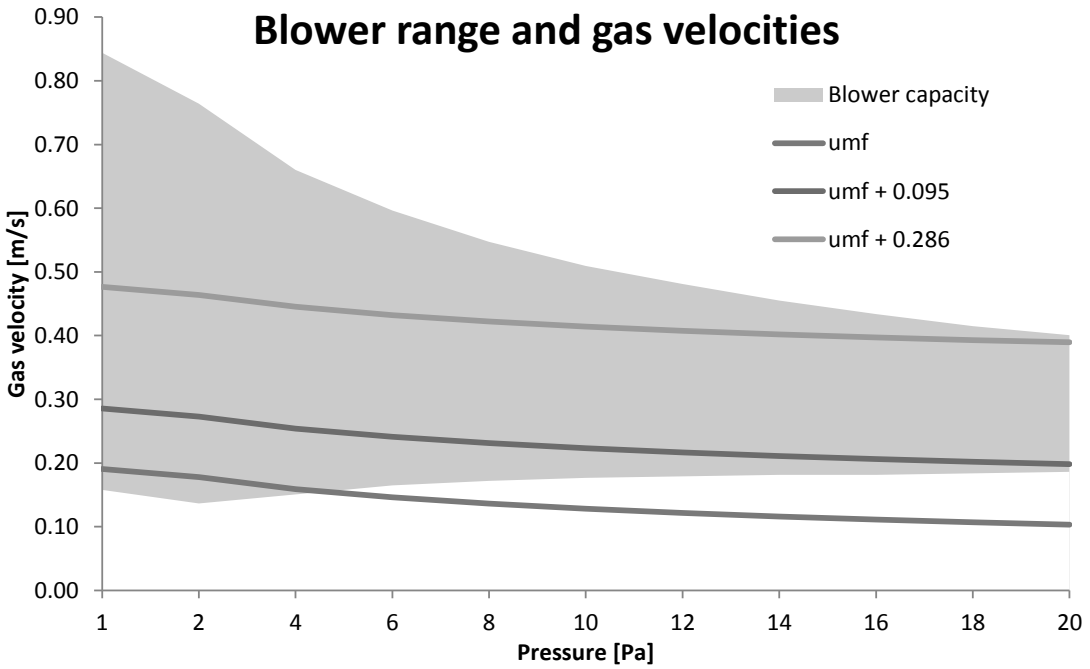

Figure 27: The blower capacity with the u_{mf} and the desired superficial gas velocities.

4.1.1 Geldart classification

The Geldart classification of particles at elevated pressures is calculated in this paragraph. At atmospheric conditions the Geldart classification can be easily calculated with help of the Archimedes number that is presented by equation (2). However in this project the fluidized bed is operating under elevated pressures. Therefore, the Geldart type is determined with help of figure 28, the Archimedes number and the dimensionless density is given by equation (6).

$$\text{Dimensionless density} = \frac{\rho_p - \rho_f}{\rho_f} \tag{6}$$

The fluidized bed operates at the border of the Gedart B/D regime. Where the fluidized bed at atmospheric conditions is more likely to be in the Gedart B regime and when the fluidized bed is operated at elevated pressures (≥ 10 bara). [16]

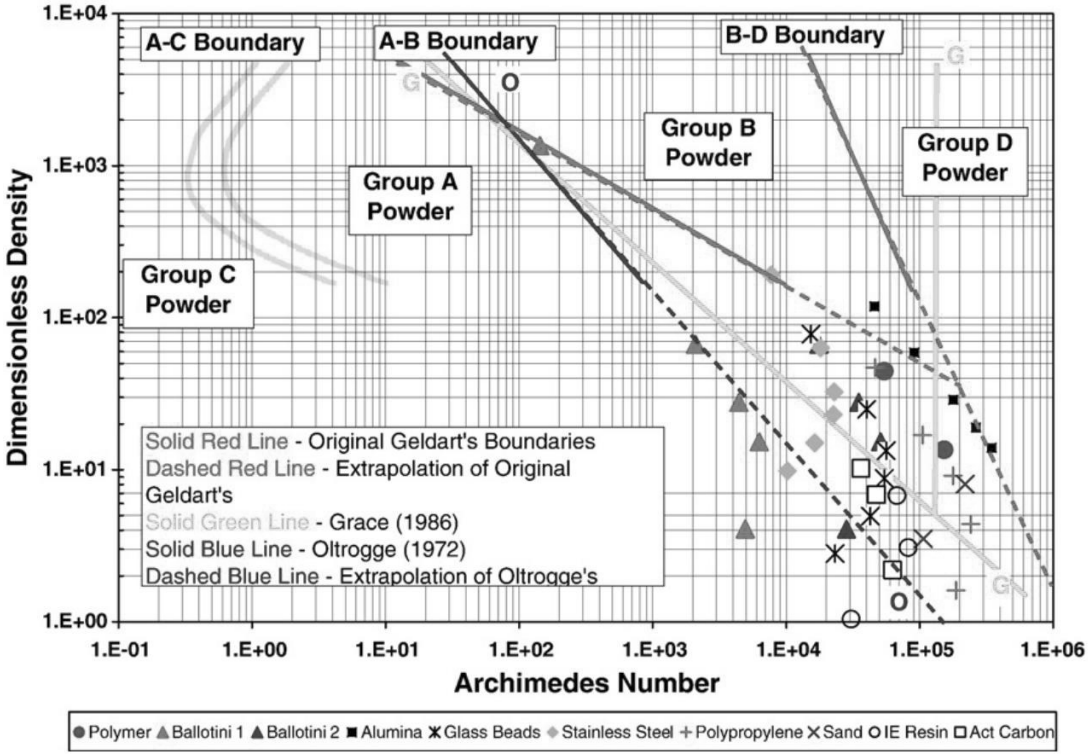

Figure 28: Geldart regimes classifications for pressurized fluidization. [16]

4.2 Results and discussion

In figure 29 the results of the experiment with low fluidization velocity is shown. Here the gas velocity was 0.095 m/s higher than the minimum fluidization velocity that was determined for the specified pressure. Experimental conditions are presented in table 26. The graph of the low fluidization pressure experiment shows an upward velocity near the center of the fluidized bed and a low or even downwards velocity for the particles near the wall of the fluidized bed. The results showed that solid velocity at the center of the bed increases with pressure.

The experiments with the high fluidization velocity are shown in figure 30. The gas velocity was 0.286 m/s above minimum fluidization in these experiments. The particles near the center are showing an upwards movement and the particles near the wall have a velocity around zero. This looks similar as the results at low fluidization velocity. Only the velocity near the center is lower and the graphs shows a more fluctuating result, compared to the low fluidization velocity. Due to the fluctuating results, it is hard to say more about these graphs.

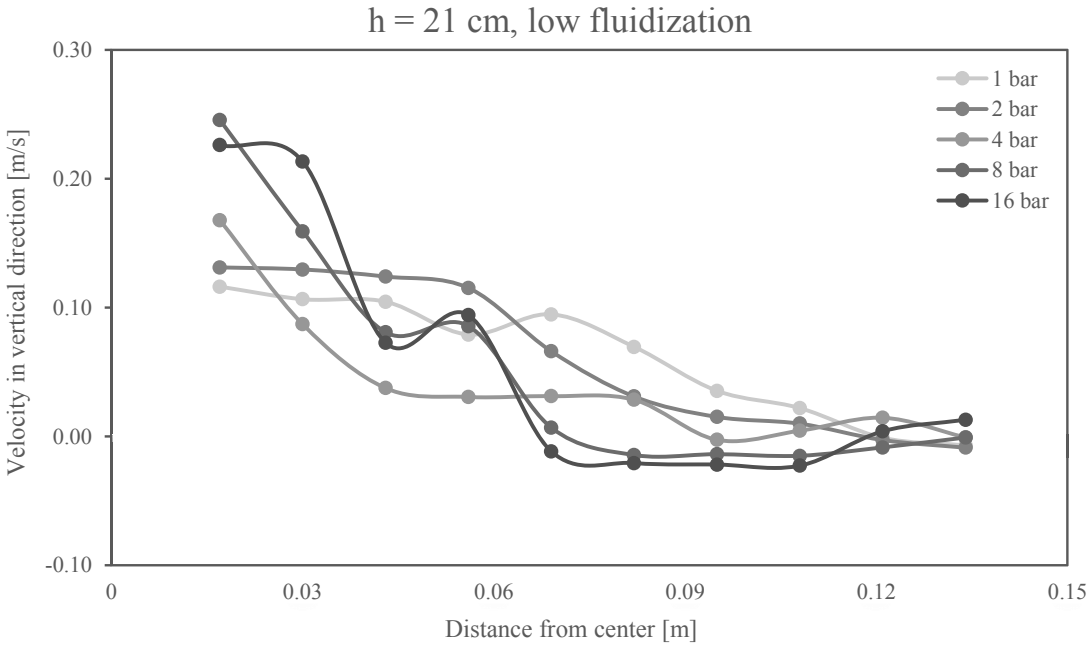

Figure 29: Effect of pressure on radial solid velocity profile at relatively low fluidization velocity.

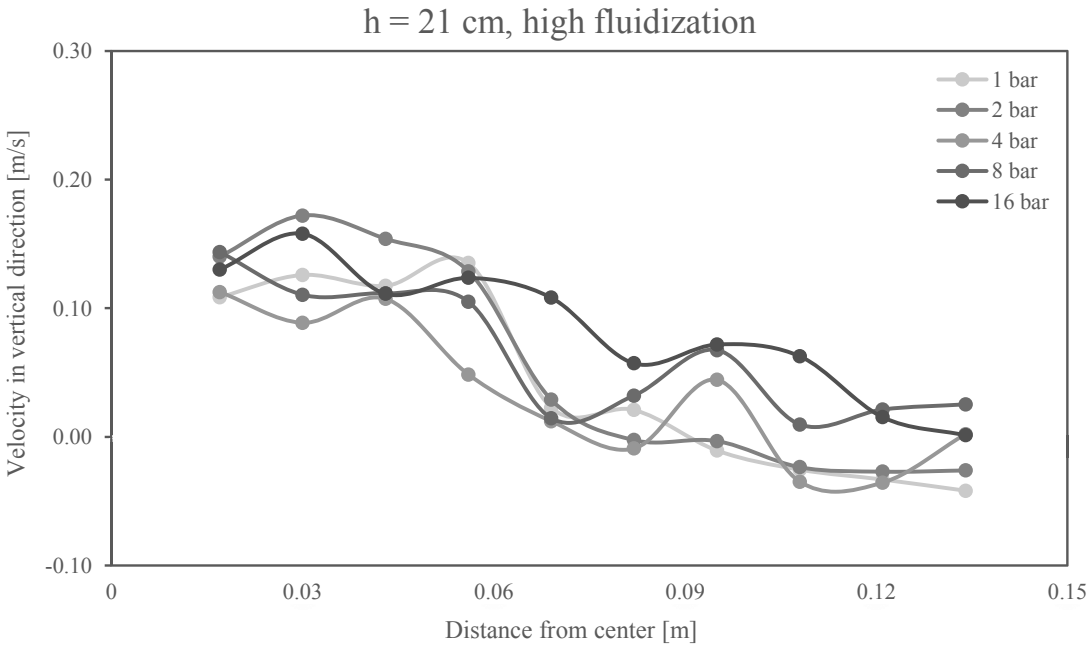

Figure 30: Effect of pressure on radial solid velocity profile at relatively high fluidization velocity.

4.3 Observations

The picture that are made during the pressure experiments are also observed with the human eye. In figure 31 snapshots are shown at different pressures, taken through the ocular. It was tried to find a snapshot with a bubble in them.

When looked at a small selection of the total 750,000 snapshots made during the pressure experiment, a couple of things were observed. In snapshots near the center of the fluidized bed an up-going movement of the particles was noticed. Where the particles near the wall of the fluidized bed were going up, down or did not moved at all. The frequency of bubbles at higher pressure was slightly higher than at lower pressures. Where the frequency of bubbles in the center was clearly a lot higher than near the wall of the fluidized bed. The frequency of the bubbles near the fluidized bed wall was so low that it was very hard to find one. On the other hand, the bubbles at the center of the fluidized bed where easy to spot.

The size of the bubbles had a variety from around 1 cm till larger than 5 cm. The larger than 5 cm bubble can be found in figure 31 at a pressure of 4 bara. The bubbles have various shapes and most of the time were not spherical. It should be noted that the snapshots in figure 31 are enhanced and have a 20% more brightness and 40% more contrast than the original snapshots. This was done to give the reader a better view.

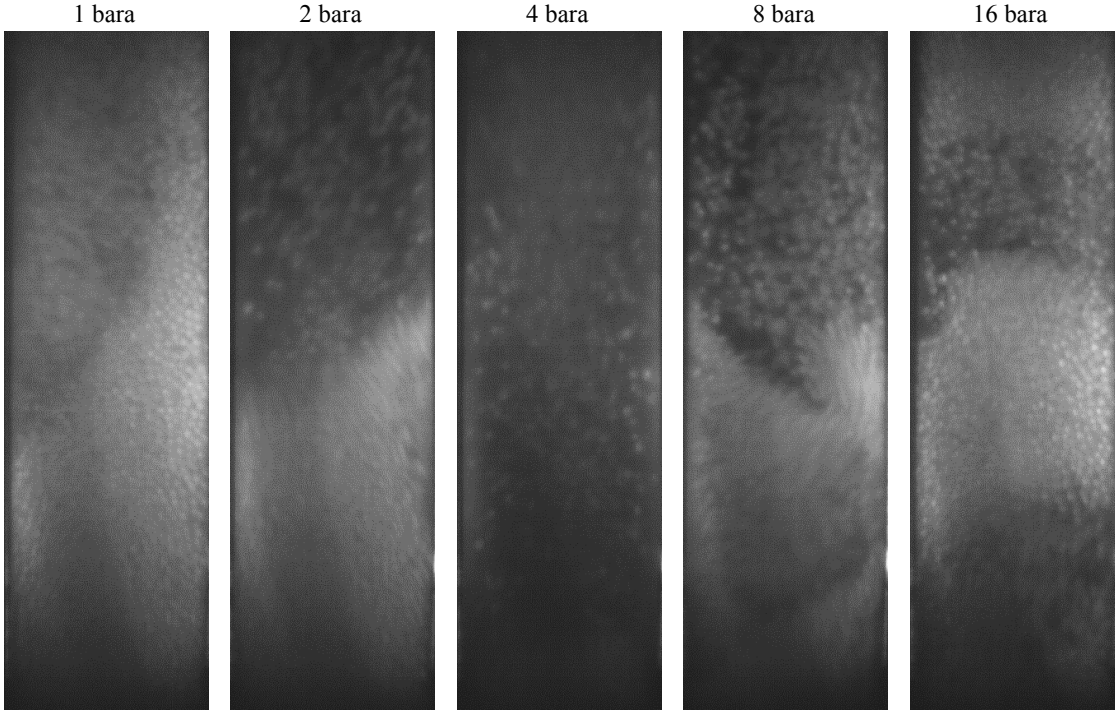

Figure 31: Snapshots taken with the ocular at low fluidization velocity near the center of the bed (position 1) at different pressures.

4.4 Literature review

Laverman [9] found similar results at atmospheric conditions. Both the magnitude and the trend of their results was similar to the obtained results in this project. Vikrant [17] also performed

some simulations with TFM at various pressures and his results and the BPIV results had similarities with each other.

4.5 Conclusion

The average particle velocity shows an up-going movement near the center of the fluidized bed and an average velocity around zero near the wall of the bed. It was found that the frequency of the bubbles near the center of the fluidized bed was much higher than its corresponding value near the wall of the fluidized bed.

5 Modeling and simulation

Focusing on experiments is a possibility in research, but when correlating with simulation models is also a possibility, this approach should also be exploited. Simulations have several advantages over experimental techniques. They are non-intrusive, relatively cheap, easy to setup and they can also give a lot of detailed information that experimental techniques cannot give us. Various models have been developed for simulating of fluidized beds. Some of these models and their scale of simulations are presented in figure 32.

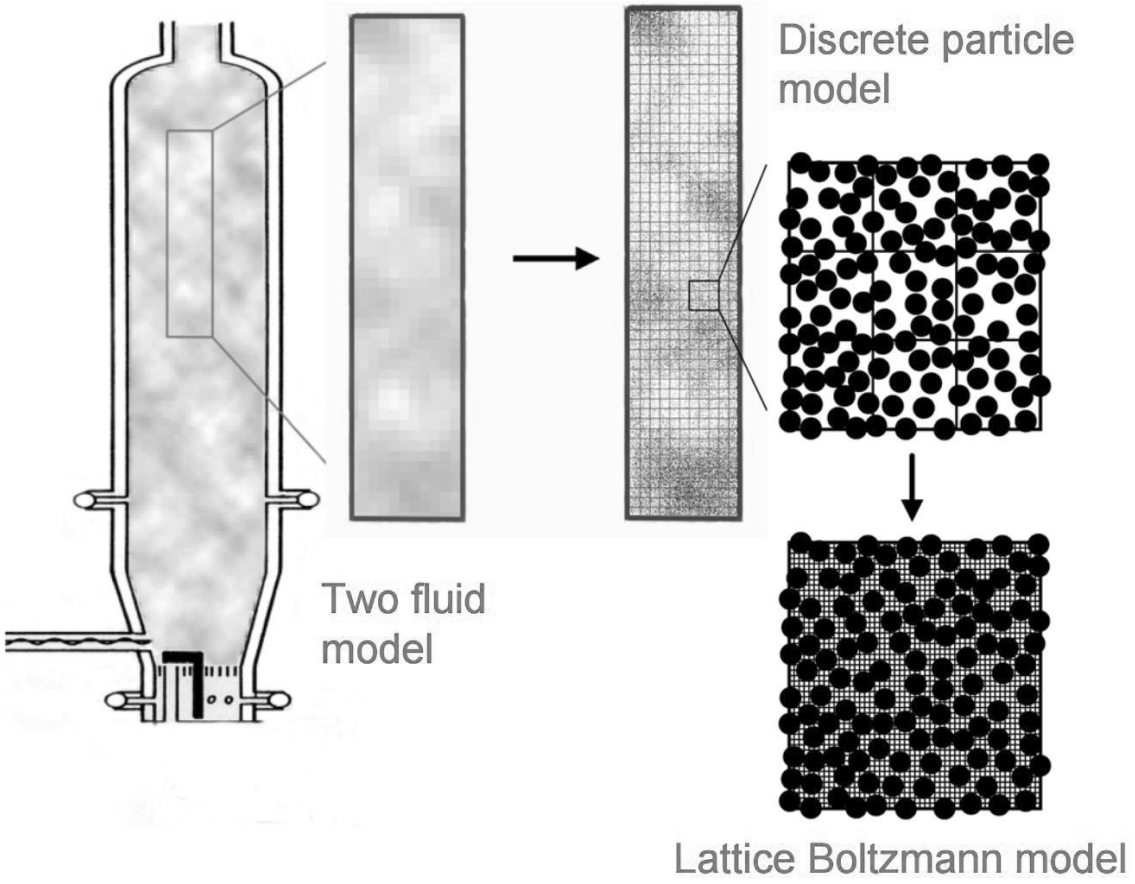

Figure 32: The TFM can simulate a large lab-scale fluidized bed, where the DPM, DNS and LBM can only simulate a part of it, but with a larger amount of details [18].

The amount of information and accuracy of simulation results depends on the chosen model. The drawback of very accurate models is the large amount of computational time that they require. Therefore, a concession has to be made between the level of accuracy and a reasonable computational time.

5.1.1 Lattice Boltzmann model

The Lattice Boltzmann model (LBM) and direct numerical simulation (DNS) are very accurate computational fluid dynamics (CFD) models that can be used for modeling of around 10^3 particles. The final results of these models can be used as a closure for larger scale models like

discrete particle model (DPM) and two fluid model (TFM). Some of the well-known drag correlations were obtained with these techniques [19].

5.1.2 Discrete particle model

The discrete particle model (DPM) is less accurate than the LBM/DNS, but is applicable for a larger scale simulations. This model is suitable for systems with maximum number of 10^6 particles with common processors. This model is an Eulerian-Lagrangian approach. In this model, every individual particle is tracked separately and all the exerting forces to these particles should be calculated at each computational time-step. On the other hand, the gas phase is considered as a continuous phase and it is governed by Navier-Stokes equations. This model is a learning model that can be used only for small lab-scale fluidized beds [20].

5.1.3 Two-fluid model

The two-fluid model (TFM) treats the gas phase as well as the particulate phase as continuous and interpenetrating phases where the individual particles are not tracked. This model is suitable for simulating of large lab-scale fluidized beds [6].

5.1.4 Discrete Bubble Model

The Discrete Bubble Model (DBM) is a model that can simulate complex hydrodynamic phenomena, which occur in large scale gas-solid fluidized beds. Where the importance of simulating lays in the macro-scale emulsion phase circulation patterns through bubble coalescence. Every bubble is registered and is modeled as a discrete element in an emulsion phase that is modeled as a continuum.
This model needs further research to enable a precise description of bubble behavior [21].

5.1.5 Conclusion

The amount of particles in the fluidized bed used in this project is around $2 \cdot 10^8$ particles. Thus, the LBM/DNS and DPM require an extremely long computational time to be used. The DBM has its limitations and need more improvement and closure in its equations. The TFM can model a bed as large as the experimental setup that has been used in this work. Therefore, this model is the most suitable model for the simulations in this project.

5.2 The two-fluid model and its governing equations

Even though TFM is much faster than DEM and DNS, the computational time with a TFM is still quite high. The different simulations that are performed for this project, took around 1 year, to simulate 10 seconds of operating time.
The TFM that was used for this project was compiled by Prof.dr.ir. J.A.M. Kuipers and Ir. M.J.V. Goldschmidt in 2000. Where the model is supported by the Kinetic Theory of Granular Flows (KTGF). This model was extended and verified for cylindrical systems by Verma [22].The governing equations of this model are as follows:

Continuity and Navier-Stokes equation for the gas phase:

$$\frac{\partial}{\partial t}(\varepsilon_f \rho_f) + \nabla \cdot (\varepsilon_f \rho_f \bar{u}_f) = 0 \tag{7}$$

$$\frac{\partial}{\partial t}(\varepsilon_f \rho_f \bar{u}_f) + \nabla \cdot (\varepsilon_f \rho_f \bar{u}_f \bar{u}_f) = -\varepsilon_f \nabla P_f - \nabla \cdot (\varepsilon_f \bar{\bar{\tau}}_f) - \beta(\bar{u}_f - \bar{u}_s) + \varepsilon_f \rho_f \bar{g} \tag{8}$$

The ideal gas law was used for correlating the gas density to its pressure and temperature.
Ideal gas law:

$$\rho_f = \frac{M_f P_f}{R T_f} \tag{9}$$

Particulate phase is also considered as a fluid. Therefore, similar governing equations are used for this phase:

$$\frac{\partial}{\partial t}(\varepsilon_s \rho_s) + \nabla \cdot (\varepsilon_s \rho_s \bar{u}_s) = 0 \tag{10}$$

$$\frac{\partial}{\partial t}(\varepsilon_s \rho_s \bar{u}_s) + \nabla \cdot (\varepsilon_s \rho_s \bar{u}_s \bar{u}_s) = -\varepsilon_s \nabla P_f - \nabla P_s - \nabla \cdot (\varepsilon_s \bar{\bar{\tau}}_s) + \beta(\bar{u}_f - \bar{u}_s) + \varepsilon_s \rho_s \bar{g} \tag{11}$$

The inter phase momentum transfer coefficient (β) is calculated with the drag relation from Wen and Yu [23] and is described in equation (12). Link et al. [2005] and Bokkers et al. [2004] used these expressions and found good results with it.

$$\beta = \frac{3}{4} 3\pi \mu_g \varepsilon^2 d_p (u - \upsilon) f(\varepsilon) \tag{12}$$

Ergun correlation:

$$f(\varepsilon) = \frac{150(1-\varepsilon)}{18\varepsilon^3} + \frac{1.75}{18} \frac{\mathrm{Re}_p}{\varepsilon^3} \tag{13}$$

Wen and Yu correlation:

$$f(\varepsilon) = \frac{C_d}{24} \mathrm{Re}_p \, \varepsilon^{-4.65} \tag{14}$$

The drag coefficient (C_d) for $Re_p < 1000$ [23]:

$$C_d = \frac{24}{\mathrm{Re}_p}(1 + 0.15 \mathrm{Re}_p^{0.678}) \tag{15}$$

The overall granular temperature (θ) has been calculated with equation (16) and is 1/3 of the average velocity fluctuation component ($\bar{C}_p$) squared, which is presented by equation (17). The granular temperature equation is described by equation(18).

$$\theta = \frac{1}{3} < \bar{C}_p \cdot \bar{C}_p > \tag{16}$$

$$\bar{c}_p = \bar{u}_s + \bar{C}_p \tag{17}$$

$$\frac{3}{2}\left[\frac{\partial}{\partial t}(\varepsilon_s \rho_s \theta + \varepsilon_s \rho_s \theta \bar{u}_s)\right] = -(P_s \bar{\bar{I}} + \varepsilon_s \bar{\bar{\tau}}_s) : \nabla \bar{u}_s - \nabla \cdot (\varepsilon_s q_s) - 3\beta\theta - \gamma \tag{18}$$

Particle pressure:

$$P_s = [1 + 2(1+e_n)\varepsilon_s g_0]\varepsilon_s \rho_s \theta \tag{19}$$

Newtonian stress-tensor:

$$\bar{\bar{\tau}}_s = -[\left(\lambda_s - \frac{3}{2}u_s\right)(\nabla \cdot \bar{u}_s)\bar{\bar{I}} + u_s((\nabla \bar{u}_s) + (\nabla \bar{u}_s)^T)] \tag{20}$$

Solid bulk viscosity:

$$\lambda_S = \frac{4}{3}\varepsilon_S \rho_S d_P g_0 (1+e_n)\sqrt{\frac{\theta}{\pi}} \tag{21}$$

Solid shear viscosity:

$$\mu_S = 1.01600\frac{5}{96}\pi\rho_S d_p \sqrt{\frac{\theta}{\pi}} \frac{(1+\frac{8}{5}\frac{(1+e_n)}{2}\varepsilon_S g_0)(1+\frac{8}{5}\varepsilon_S g_0)}{\varepsilon_S g_0} + \frac{4}{5}\varepsilon_S \rho_S d_p g_0 (1+e_n)\sqrt{\frac{\theta}{\pi}} \tag{22}$$

Pseudo-Fourier fluctuating kinetic energy flux:

$$\bar{q}_S = -\kappa_S \nabla \theta \tag{23}$$

Pseudo-thermal conductivity:

$$\kappa_S = 1.02513\frac{75}{384}\pi\rho_S d_p \sqrt{\frac{\theta}{\pi}} \frac{(1+\frac{12}{5}\frac{(1+e_n)}{2}\varepsilon_S g_0)(1+\frac{12}{5}\varepsilon_S g_0)}{\varepsilon_S g_0} + 2\varepsilon_S \rho_S d_p g_0 (1+e_n)\sqrt{\frac{\theta}{\pi}} \tag{24}$$

Dissipation of granular energy due to inelastic particle-particle collisions:

$$\gamma = 3(1-e_n^2)\varepsilon_S^2 \rho_S g_0 \theta [\frac{4}{d_p}\sqrt{\frac{\theta}{\pi}} - (\nabla \cdot \bar{u})_S)] \tag{25}$$

Radial distribution function:

$$g_0 = \frac{1 + \varepsilon_S(\varepsilon_S(4.5904 + 4.515436\varepsilon_S))}{\left(\frac{1-\varepsilon_S^3}{\varepsilon_{S,\max}^3}\right)0.678202} \tag{26}$$

The settings that are used for simulating the TFM can be found in table 25, table 26 and

table 27. In figure 33 some snapshots from a slice at the center of the bed is shown at various operating pressures.

Table 25: The TFM settings that are used for simulations during this project.

TFM setting	Value
Pressure (P)	1, 2, 4, 8, 16 [bara]
Gravity (g)	9.80 [m/s^2]
Molar mass (M)	0.02802 [kg/mol]
Temperature (T)	298.0 [K]
Shear viscosity	1.83×10^{-5} [Pa·s]
Particle density (ρ_p)	2,500 [kg/m^3]
Time step (t)	5×10^{-5} [s]
Number of cycles	200,000 [-]
Running time	10 [s]
Size of cells in x-direction	0.0015 [m]
Size of cells in y-direction	0.209 [rad]
Size of cells in z-direction	0.0015 [m]
Number of cells in x-direction	100
Number of cells in y-direction	30
Number of cells in z-direction	300
Diameter particle (d_p)	5×10^{-4} [m]
Gas particle drag correlation	Ergun + Wen&Yu [24]
Aspect ratio	0.5
Kinetic theory	KTGF St.Annaland 1th order Enskog method
Flux Limiter function discretization Scheme	SUPERBEE
Superficial gas velocities	Table 23
Restitution coefficient	0.97

Table 26: Initial conditions used in the TFM simulations.

Initial TFM settings	Value
Initial granular temperature for all particles	0.001 [m^2/s^2]
imin	1
imax	100
jmin	1
jmax	30
kmin	1
kmax	100
Gas volume fraction	0.40
Maximum random relative fluctuation on initial volume fractions	1.0 [%]

Table 27: Boundary conditions used in the TFM simulations.

TFM Boundary settings	Value
Cellflag left wall / inner radius	Free-slip for gas and particles
Cellflag right wall / outer radius	No-slip for gas and partial-slip for particles
Cellflag front wall / min angle	Periodic boundary condition
Cellflag back wall / max angle	Periodic boundary condition
Cellflag bottom	Prescribed influx for gas and particles
Cellflag top	Prescribed pressure for gas and impermeable no slip for particles

For more details about KTGF, an interested reader is referred to the work by Goldschmidt et al. [25].

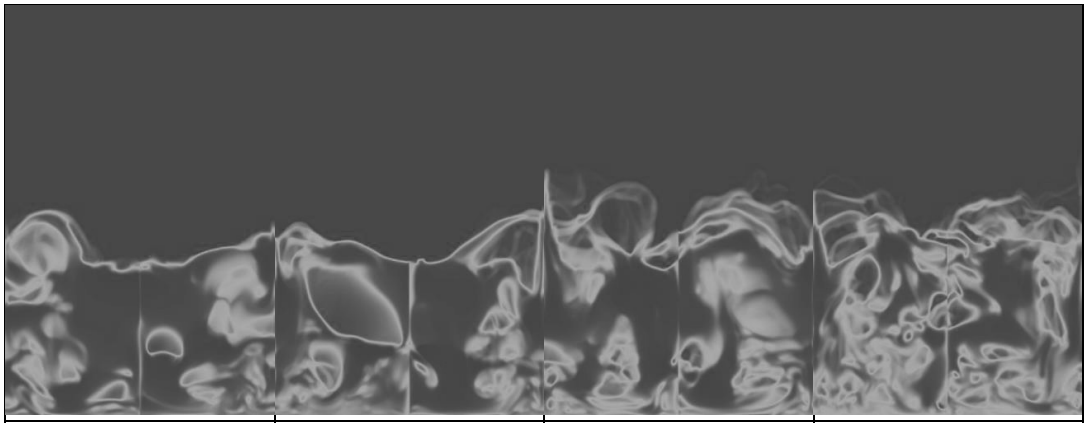

Figure 33: Some snapshots on the effect of pressure on fluidization behavior (u_0= u_{mf} + 0.286 m/s). These snapshots only show a slice in the bed center.

5.3 Results and discussions

In this chapter the results of the simulations at $u_0 = u_{mf} + 0.95$ m/s and various pressures are presented. In figure 34 the gas fraction and its probability distribution function (PDF) are displayed. Where the most PDF is at the emulsion phase, which is between 0.4 and 0.5. Here a higher pressure results in a lower peak in the emulsion phase and a higher distribution in the intermediate phase. The PDF equation is displayed in equation (27). Where V = the volume of cell and S = the cells that have a gas fraction between $\varepsilon_i < \varepsilon_s < \varepsilon_{itl}$.

$$PDF_i = \frac{\sum_{k \in S} V_k \cdot \rho_k}{\sum_{k \in dense\,zone} V_k \cdot \rho_k} \tag{27}$$

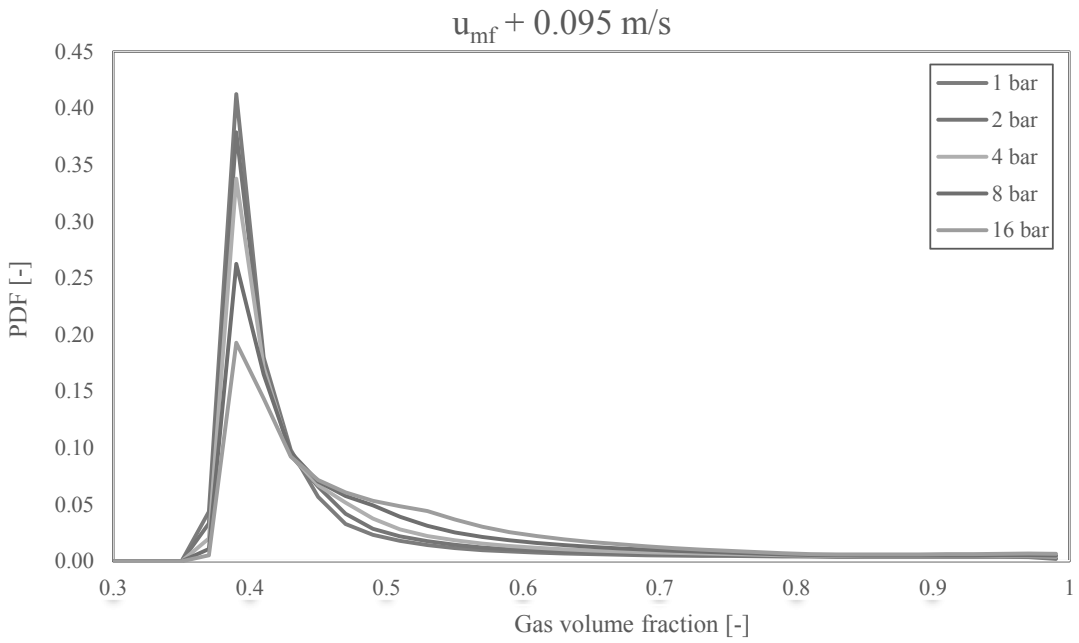

Figure 34: Gas fraction and its PDF at different pressures.

Figure 36 displays the average gas fraction at different heights from the distributor. The average gas fraction here is around 0.5 and the freeboard starts around a height of 0.2 m. It can be seen that a larger pressure results in a larger gas fraction and a larger average bed height.

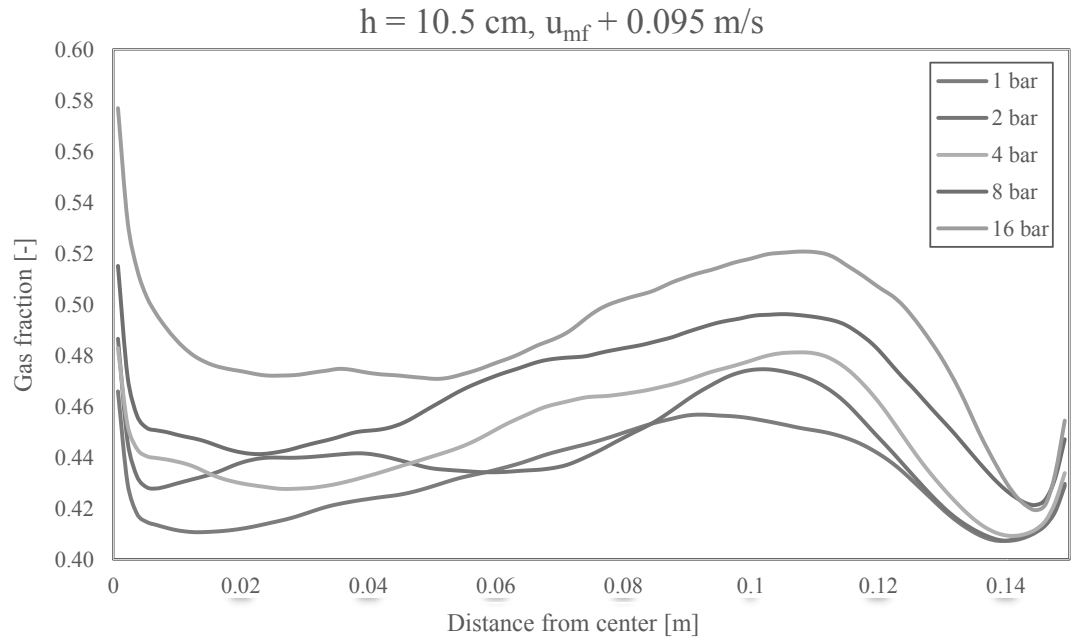

Figure 35: Gas fraction at distance from center at different pressures.

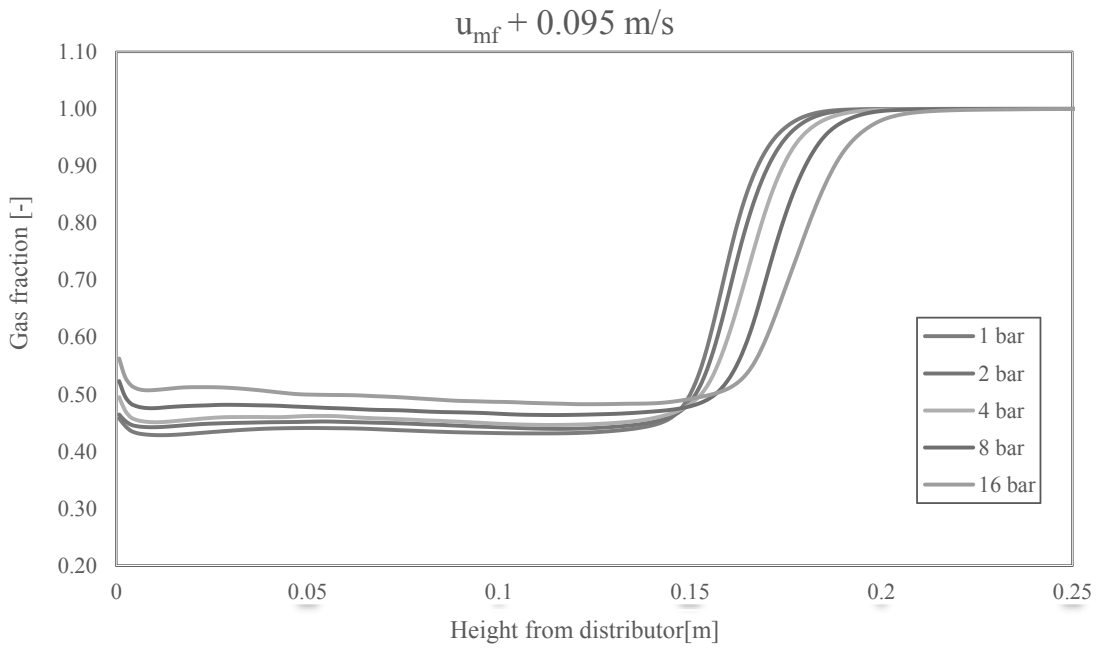

Figure 36: The effect of pressure on axial gas volume fraction profile.

Figure 35 shows the gas fraction at a height of 10.5 cm above the distributor. A higher pressure results in a higher gas fraction.

In figure 37 the particle velocity at a height of 10.5 cm above the distributor is displayed versus the distance from the center. It seems that the particle velocity in the center is negative where at a distance of 0.1 m from the center the particle velocity peaks in going up. Near the wall, the particle velocity peaks in a downward velocity, where close to the wall the particle velocity becomes zero due the wall friction. A higher pressure results in larger peaks in both up going and down going particle velocities. Laverman [9] found similar results at a height of 11.0 cm at atmospheric conditions for both the magnitude as the trend. Only the wall effect was less noticeable in his results and therefore showed a down-word movement for the particles very close to the wall.

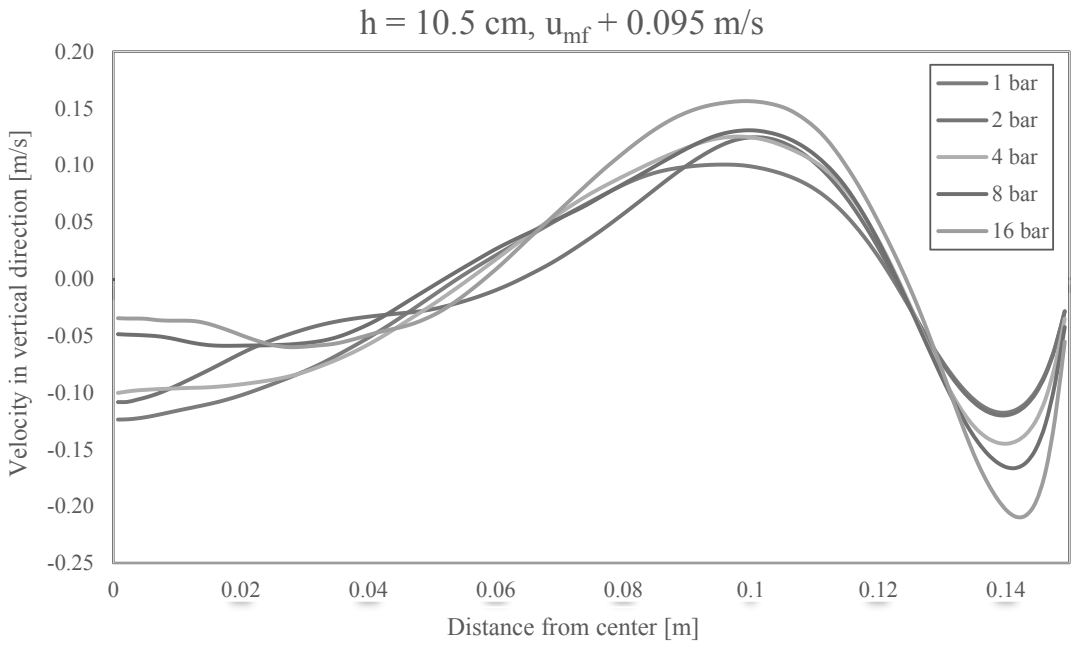

Figure 37: Radial profile of average solid velocity at different pressures.

5.4 Conclusion

The TFM results showed comparable to the results in open literature. Most of the gas fraction had a distribution in the emulsion phase, which is between a gas fraction of 0.4 and 0.5 and the average gas fraction was around 0.5. The emulsion phase was smaller at higher pressures. The freeboard starts around a height of 0.2 m and the average bed height increases with pressure. The average gas fraction at a height of 10.5 cm is lower near the wall than around the center. It was also found that, a higher pressure leads to a higher gas fraction.

The average particle velocity shows a negative velocity in the center and near the wall, were between the center and the wall the average particle velocity was positive. This results are different from the experimental observations which can be due to different aspect ratio in the simulations and experiments. As the simulation with an aspect ratio of 0.5 and experimental settings with an aspect ratio of 1.0 are not the same, it is not possible to compare their results to each other.

6 Conclusions

A novel BPIV technique is validated with performing various experimental tests. It is found that this technique can be used for solid velocity measurement in bubbling gas-solid fluidized beds. Besides the validation part, the best settings for using of this technique was obtained. It is found that 1000 FPS image capturing settings and minimum 7.5 s of measurement give the best results. It is also realized that the light source and particle light reflectivity have a significant effect on the final BPIV results. For this reason, it is necessary to use particles with high light reflectivity and the highest possible illumination power in the experiments. It was also discovered that particles that are painted may make the oculus dirty and consequently affect the measurements.

The fluidized bed and corresponding distributor in this project are validated and they are working properly now and they can be operated safely up to a pressure of 16 bara.

In the performed experiments, the particle velocity in the center shows an average up going velocity up to a maximum of approximately 0.25 m/s, where near the wall the average vertical velocity was around zero m/s.

The trend of solid velocity profile is clearer at low fluidization velocities compared to the similar trend at high fluidization velocities. This is due to the high level of fluctuations in the final BPIV results at high fluidization velocity conditions.

Besides the experimental part of this project, the two fluid model was also used for finding the effect of pressure on fluidization. After processing the results, it is found that the TFM gives comparable outcomes to the existing results in open literature. It was found that the operating pressure change the fluidization behavior. As the simulation and experimental settings were not the same, it was not possible to compare their results to each other.

7 Recommendations

Now that the borescope is validated, proven to be useful and the best settings are known. The borescope can be used in a lot of other experiments.
The same experiments can be repeated at a different height for example 31 cm above the distributor or with different particles (preferably white particles without paint, for example polyethylene particles).
The solid volume fraction can be calculated and the results can be incorporated into BPIV analysis. For this purpose a black box with lots of holes in its sides was made. This box is made in a way that the ocular can fit into it. It is possible to put a desired number of particles (beads) into this box, like figure 38. After taking some images from the black box with particles in it, it is possible to find the correlation between image intensity and the solid volume fraction.

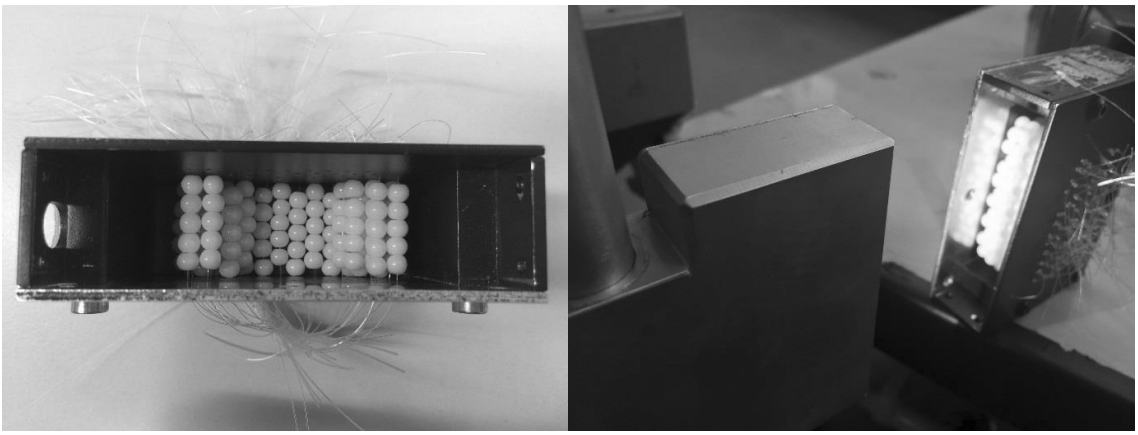

Figure 38: Left: Black box partially filled with particles. Right: Black box in front of the ocular.

The TFM can be redone with a bed height of 30 cm. So these results can be compared with the experiments of this project. The required files are already configured and they can be started and run for approximately one year. It is also possible to simulate a fluidized bed with the borescope inside of the fluidized bed to check the intrusiveness of the endoscope in the TFM.

Acknowledgements

Finishing my master program was an interesting challenge for me, but I was lucky enough to have a lot of people who helped me with this big task. Without these people, I could definitely not create this report or even finish my master education. Therefore, I would like to thank these people in this chapter.

First I would like to thank my supervisor Mohammad Banaei MSc. We had a lot of helpful, critical and philosophical discussions, heavy labor and he provided me with a lot of good feedback on my report. I also wish him good luck with finishing his PhD and I hope that I can come and have a coffee with him in the future.

I would also like to thank prof. dr. ir. Hans Kuipers for making it possible to do my master thesis in the Multi-scale Modelling of Multi-phase Flows group and for the feedback and ideas he provided.
Furthermore, I would like to thank prof. dr. ir. Niels Deen for helping me with my project, especially about sharing his knowledge about the DaVis program. I wish him good luck with his newly obtained group, Multiphase & Reactive Flows.
I would also like to thank prof. dr. Jan Meuldijk. Even after the start of his retirement, he is still part of the graduation committee. I wish him a nice retirement time.

Also the students in the SMR room helped me with my report in a social and critical way. During the coffee breaks and problems with my project, they were always there. I would like especially: Jeroen Jegers, Rhea van Gijzel, Sander Hochstenbach, Tom Janssen, Floris Hieselaar, Jan Willem Oortwijn, Michel van Etten, Max Kuiper, Annelies Grijsbach, Beatrice Marinello MSc and Martin Teley.

My special thanks to my parents, Kitty Dellaert and Frans Dellaert, that made my educations financially possible, doing a lot of my laundry and their well-meant worries. I would also like to thank my grandparents, Richard Vanhijfte and Giselle Vanhijfte for their interest in my project and my master program.

During my master program, I have also received a lot of support from fellow students. Therefore, I would like to thank Robin Dellaert MSc, Joris Malcontent MSc, Rashad Rafeh MSc, ing. Sander Haers and Paulus Hamstra MSc, especially for their help in the course “Lineaire algebra” and “Calculus”.

For my big gaming hobby I would like to thank the gaming clan The Flying Dutchman (TFD), with the next active members: Rob Nieuwenhuijze, ing. Rick Claessens, ing. Thomas van Hoeve, ing. Jack Becu, Martin de Quelerij, Richard Roos and Robin Dellaert MSc. For my sporting hobby I would like to thank the football club E.S.V.V. Pusphaira.

At last I would like to thank Jurjen Pater and Astrid Almekinders for their social support and the great parties we had together.

Bibliography

[1] "Fluidized bed reactor." [Online]. Available: https://en.wikipedia.org/wiki/Fluidized_bed_reactor.

[2] "The Fluidized Bed Reactor Page," 1990. [Online]. Available: http://faculty.washington.edu/finlayso/Fluidized_Bed/index.htm#index.

[3] O. L. D.Kunii, "Fluidization engineering - second edition." 1991.

[4] J. Link, *Development and validation of a discrete particle model of a spout-fluid bed granulator*. 2006.

[5] J. Van Der Schaaf, J. C. Schouten, and C. M. Van Den Bleek, "Origin, propagation and attenuation of pressure waves in gas-solid fluidized beds," *Powder Technol.*, vol. 95, no. 3, pp. 220–233, 1998.

[6] W. Godlieb, *High Pressure Fluidization*. 2010.

[7] S. Goter, N. Deen, W. Godlieb, and J. A. M. Kuipers, "An electrical capacitance tomography study of pressurized fluidized beds," *Agglom. Dur. Fluid. Combust. Biomass*, 2010.

[8] B. P. B. Hoomans, J. a. M. Kuipers, W. J. Briels, and W. P. M. van Swaaij, "Discrete particle simulation of bubble and slug formation in a two-dimensional gas-fluidised bed: A hard-sphere approach," *Chem. Eng. Sci.*, vol. 51, no. 1, pp. 99–118, 1996.

[9] J. A. Laverman, *On the hydrodynamics in gas polymerization reactors*. 2010.

[10] S. Tebianian, K. Dubrawski, N. Ellis, R. A. Cocco, R. Hays, S. B. Reddy Karri, T. W. Leadbeater, D. J. Parker, J. Chaouki, R. Jafari, P. Garcia-Trinanes, J. P. K. Seville, and J. R. Grace, "Comparison of particle velocity measurement techniques in a fluidized bed operating in the square-nosed slugging flow regime," *Powder Technol.*, 2015.

[11] T. T. Hoeben, "Hydrodynamics of pressurized gas fluidized beds," no. September, 2014.

[12] A. M. Oldeman, "Experimental investigation of gas fluidized beds using endoscopic particle image velocimetry," no. June, 2015.

[13] "4505-427-WI Pearl Ice." [Online]. Available: http://www.sigmund-lindner.com/fileadmin/user_upload/downloads/musterkarten/20140808/Glitter_Deco_Beads.pdf.

[14] M. Size and C. Colouring, "Product Data Sheet Manufacturer / Supplier : Sigmund Lindner GmbH Oberwarmensteinacher Strasse 38 Germany Phone : ++ 49-9277-9940 Fax : Web : Company Sigmund Lindner GmbH has established a Quality Management System according DIN EN ISO 9001 since 1997 . R," pp. 2–5, 2015.

[15] A. E. C. Varas, E. A. J. F. Peters, N. G. Deen, and J. A. M. Kuipers, "Solids Volume Fraction Measurements on Riser Flow Using a Temporal-Histogram Based DIA

Method," vol. 00, no. 00, 2016.

[16] W.-C. Yang, "Modification and re-interpretation of Geldart's classification of powders," *Powder Technol.*, vol. 171, no. 2, pp. 69–74, 2007.

[17] Vikrant, *Cylindrical Fluidized Beds*. .

[18] M. Van Der Hoef, M. Ye, R. Beetstra, C. Zeilstra, and H. Kuipers, "Multi-level modeling of gas-fluidized beds," pp. 1–39, 2000.

[19] X. He and L. Luo, "Lattice Boltzmann model for the incompressible Navier–Stokes equation," *J. Stat. Phys.*, vol. 88, pp. 927–944, 1997.

[20] N. G. Deen, M. Van Sint Annaland, M. A. Van der Hoef, and J. A. M. Kuipers, "Review of discrete particle modeling of fluidized beds," *Chem. Eng. Sci.*, vol. 62, no. 1–2, pp. 28–44, 2007.

[21] G. A. Bokkers, *Multi-level modelling of the hydrodynamics in gas phase polymerisation reactors*, vol. Ph. D. 2005.

[22] V. Verma, N. G. Deen, J. T. Padding, and J. a M. Kuipers, "Two-fluid modeling of three-dimensional cylindrical gas-solid fluidized beds using the kinetic theory of granular flow," *Chem. Eng. Sci.*, vol. 102, no. OCTOBER 2013, pp. 227–245, 2013.

[23] M. Ye, J. Wang, M. a. van der Hoef, and J. a M. Kuipers, "Two-fluid modeling of Geldart A particles in gas-fluidized beds," *Particuology*, vol. 6, no. 6, pp. 540–548, 2008.

[24] N. Yang, W. Wang, W. Ge, and J. Li, "CFD simulation of concurrent-up gas–solid flow in circulating fluidized beds with structure-dependent drag coefficient," *Chem. Eng. J.*, vol. 96, no. 1–3, pp. 71–80, Dec. 2003.

[25] M. J. V Goldschmidt, J. a M. Kuipers, and W. P. M. Van Swaaij, "Hydrodynamic modelling of dense gas-fluidised beds using the kinetic theory of granular flow: Effect of coefficient of restitution on bed dynamics," *Chem. Eng. Sci.*, vol. 56, no. 2, pp. 571–578, 2001.